Proximal to distal grain-size distribution of basin-floor lobes: A study from the Battfjellet Formation, Central Tertiary Basin, Svalbard

Spychala, Y.T.[1*], Ramaaker, T.A.B.[1], Eggenhuisen, J.T.[1], Grundvåg, S.-A.[2], Pohl, F.[1+], Wroblewska, S.[3]

[1] *Department of Earth Science, Utrecht University, 3584 CB, Utrecht, Netherlands*

[2] *Department of Geosciences, UiT – The Arctic University of Norway, PO Box 6050 Langnes, N-9037 Tromsø, Norway*

[3] *Faculty of Geology, University of Warsaw, Żwirki i Wigury 93, 02-089 Warsaw, Poland*

**now at: Leibniz University Hannover, Institute of Geology, Callinstr. 30, 30167 Hannover, Germany*

[+]*now at Durham University, Department of Earth Sciences, Stockton Road, Durham DH1 3LE, UK*

Corresponding author: spychala@geowi.uni-hannover.de

thymenramaaker@hotmail.com

J.T.Eggenhuisen@uu.nl

sten-andreas.grundvag@uit.no

florian.pohl@durham.ac.uk

sara.m.wroblewska@gmail.com

twitter handles: @IvyTheSpy, @Moving_Sand, @PlasticSediment, @s_wroblewska

---

This paper is a non-peer reviewed preprint submitted to EarthArXiv and has been submitted for publication in *The Depositional Record*.
As this manuscript still has to undergo peer-review subsequent versions may have different content. If accepted, the final version of this manuscript will be available via the 'Peer-reviewed Publication DOI' link on the righthand side of this webpage. Please feel free to contact the corresponding author directly regarding this manuscript.

Abstract

The grain-size distribution of sediment particles is an important aspect of the architecture of submarine fans and lobes. It governs depositional sand quality, and reflects distribution of particulate organic carbon and pollutants. Documenting the grain-size distribution of these deep-marine sedimentary bodies can also offer us an insight in the flows that deposited them. Submarine lobes are commonly assumed to linearly fine from an apex, meaning there should be a proportional relation between grain size and distance from the lobe apex. However, not much detailed quantitative work has been done to test this hypothesis. Exposure of a 5 km long dip-section of basin-floor lobes in Clinoform 12, Battfjellet Formation, Spitsbergen, enable the study of basinward grain-size evolution in lobe deposits. Furthermore, the dataset allows testing if there are any documentable grain-size differences between lobe sub-environments.

For this purpose, the palaeogeography of Clinoform 12 was reconstructed and the youngest lobe, which was exposed in all collected logs, chosen to be evaluated for its grain-size trends. Photographed thin-sections of 66 rock samples were analysed to obtain quantitative grain-size distributions. The results show that fining of lobe deposits occurs predominantly in the most proximal and most distal parts of the lobe, while the intermediate lobe, which is dominated by lobe off-axis deposits, is characterized by a relatively consistent grain-size range. Lobe sub-environments show statistically distinct grain-size distributions from lobe axis to lobe fringe. An explanation for these trends is the interplay of capacity and competence-driven deposition with the grain-size stratification of the flows.

The outcomes of this study help to better understand the proximal to distal evolution of turbidity currents and their depositional patterns. They also provide important insights in reservoir potential of basin-floor fans at lobe scale.

Keywords

flow processes, turbidites, palaeo-reconstruction, grain-size counting, thin sections

Introduction

Grain-size distribution is one of the fundamental attributes of facies properties. It reflects transport history and depositional mechanisms of sedimentary deposits. While fine-grained turbidite systems

are characterised by larger depositional systems, longer run-out distances and larger flow sizes, coarse-grained systems are dominated by smaller depositional systems, shorter run-out systems and smaller flow sizes (Reading & Richards, 1994; Bouma, 2000). Grain-size distribution of deep-marine bodies not only govern deposit characteristics like porosity and permeability (Porten et al., 2016), but is also thought to be associated with the distribution of organic carbon (Burdige, 2005; Hedges et al.,1997) and pollutants such as plastics (Kane and Clare, 2019; Pohl et al., 2020). However, the processes that control the grain-size distribution across submarine fans are poorly understood. The root of this poor understanding seems to stem at least in part from the paucity of documentation of quantitative grain size distribution in natural submarine fan deposits (Kane et al., 2017; Fildani et al., 2018; Bell et al., 2018).

Recent studies (Straub et al., 2012; Paolo & Martin, 2012; Jobe et al., 2017; De Leeuw et al., 2018) do show that grain size changes continuously over deep-marine turbidite systems through partitioning along channel-levee complexes. This grain size partitioning governs the range of grain sizes that is transferred to basin-floor lobe complexes (De Leeuw et al., 2018). In general, studies suggest that the largest amount of sand within a shelf-slope-basin floor system is located within the basin-floor deposits (e.g.Hubbard et al., 2014; van der Merwe et al., 2014; Prather et al., 2017; Bell et al., 2018), and that lobe deposits are also relatively coarse compared to the correlative channel-levee deposits (de Leeuw et al., 2018). The fact that basin-floor deposits are coarser grained than their coeval channel-levee deposits is explained by the stratification of flow where fining upwards within the flow hampers the loss of coarser material from the channel thorugh overspill while increasing the loss of finer grains.

While we understand the relationship between lobes and the rest of the deep-marine system we know very little about the grain-size distribution within the lobes themselves. Sylvester and Lowe's (2004) study of vertical fining patterns within turbidites and hybrid beds was one of the first detailed study of grain-size distribution within lobe deposits and the processes that formed them. More recently, Fildani et al. (2018) looked into detailed vertical grain-size distributions within different bed types attributed to turbidites, hybrid beds and debrites using laser particle analysis. Their study suggests that turbidite deposits in lobes contain more silty material than estimated from visual core description alone, underlining the need for integration of macroscopic facies analysis with microscopic analysis to inform more comprehensive depositional models. Bell et al. (2018) looked into longitudinal trends of grain-size distribution within lobes from the Gerbe system (Aínsa Basin, Spain) in more detail. They observed that lobe sub-environments (lobe axis, lobe off-axis, lobe fringe and lobe distal fringe; *sensu* Prélat et al., 2009) show a longitudinal decrease in mean grain-size from lobe axis to fringe, but couldn't report a specific trend. Instead, they documented that for the Gerbe

system down-dip decrease in grain size between lobe axis and off-axis is minimal, whereas a more distinct decrease can be documented down-dip between lobe off-axis and fringe deposits.

The aim of this integrated outcrop and grain-size study is to assess the longitudinal trend of grain-size distribution from inferred axial to fringe lobe deposits. For this purpose, we are using sandstones preserved in the basin-floor segment of Clinothem 12 (sensu Steel & Olsen, 2002) of the Battfjellet Formation (Central Tertiary Basin, Svalbard) at Storvola and Hyrnestabben, which previously have been interpreted as basin-floor fan deposits (Steel & Olsen, 2002; Crabaugh & Steel, 2004; Johannessen & Steel, 2005). The specific research objectives are: 1) detailed reconstruction of facies, architecture and hierarchy of the exhumed lobe deposits, 2) analysis of grain-size differences between lobe sub-environments, and 3) assessment of the longitudinal trend of grain-size distribution of the youngest exposed lobe. The documented spatial trends in grain size within and between the lobe sub-environments provide a basis to discuss flow processes of turbidity currents flowing over and depositing lobes. Gained insights could be used in future process modelling of lobe deposits.

Geological Setting

The Central Tertiary Basin (CTB) is located on southwest Spitsbergen, the largest island of the Svalbard archipelago, Arctic Norway (Fig. 1A). The basin formed during the Paleocene and early Eocene contemporaneous with the formation of the West Spitsbergen Fold and Thrust Belt (WSFTB), which is located along the western edge of Spitsbergen and closely linked to the strike-slip opening of the Norwegian-Greenland Sea and later sea floor spreading (Kellogg, 1975; Steel et al., 1985; Helland-Hansen, 1990; Müller & Spielhagen, 1990; Lundin & Dore, 2002; Helland-Hansen & Grundvåg, 2020). Dextral shearing and subsequent transpression/compression along the De Geer Shear Zone caused by the northward movement of Greenland resulted in crustal shortening and thrusting-up of the WSFTB (Myhre et al., 1982; Müller & Spielhagen, 1990; Leever et al., 2011). The initial phase possibly started in the Late Cretaceous or early Paleocene with oblique contraction and possibly reversion of N–S normal faults in eastern Spitsbergen (Haremo and Andresen, 1992) and was followed by the main phase of ENE-oriented contraction during latest Paleocene–Eocene (e.g. Steel et al., 1985; Braathen et al., 1995; Bergh et al., 1997; Bruhn and Steel, 2003). Some authors have linked the WSFTB to the Eurekan fold belts of North Greenland and Arctic Canada (e.g. Piepjohn et al., 2016). The NNW–SSE oriented CTB is located east of the orogenic belt (i.e. the

WSFTB) and is identified as a foreland basin despite its connection to the bordering transpressive orogeny (Helland-Hansen, 1990; Bruhn and Steel, 2003; Helland-Hansen and Grundvåg, 2020).

The CTB comprises the c. 2.3 km thick Van Mijenfjorden Group, which was deposited from the early Paleocene to the Eocene and possibly early Oligocene (Fig. 1B). Sediments of the Paleocene Firkanten, Basilika and Grumantbyen Formations were delivered from the east, before a regional drainage reversal occurred at the transition from the late Paleocene to the early Eocene (Steel et al., 1981; Petersen et al., 2016). Subsequent formations (the Hollendardalen, Frysjaodden, Battfjellet and Aspelintoppen Formations) were fed from the emerging orogenic wedge located to the west (Steel et al., 1981; 1985; Helland-Hansen, 1990; Petersen et al., 2016). This study will focus on the slope to basin-floor sediments of the Eocene Battfjellet Formation.

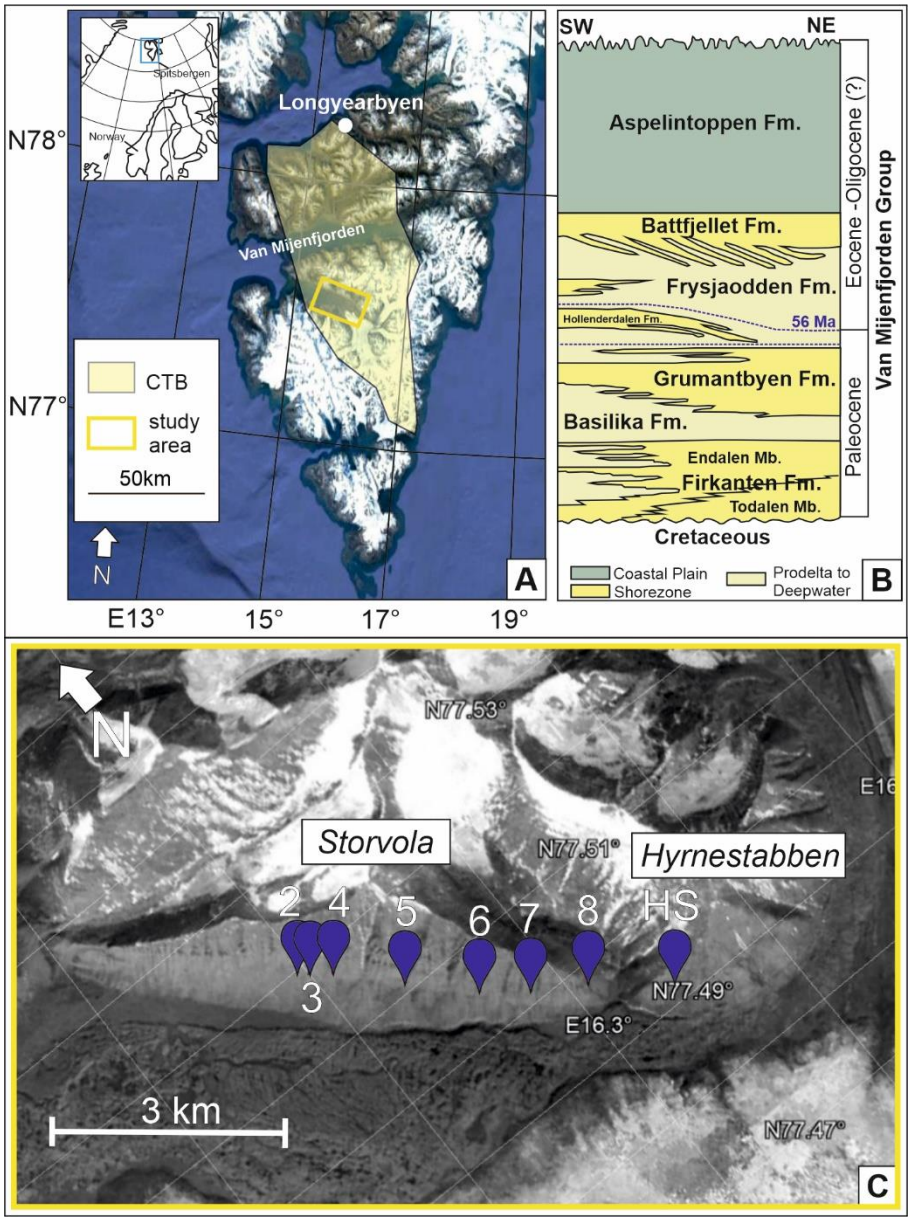

Fig. 1: A) Location of the Central Tertiary Basin (CTB). The square indicates the location of the study area in the Van Keulenfjorden. B) Stratigrpahy of the CTB (modified from Crabaugh and Steel, 2004). The Battfjellet Formation is interpreted to be of Eocene to Oligocene age. C: Location of outcrop sections along Storvola and Hyrnestabben used in the study. Satellite images are taken from Google Earth.

Battfjellet Formation and Clinothem 12

The Eocene Battfjellet Formation comprises a series of clinothems that migrated eastwards into the foreland basin (Steel et al., 1985; Helland-Hansen, 1990, 1992; Helland-Hansen and Grundvåg, 2020). Present dip angles for the associated clinoforms are in the range of 1–4°, and have not been decreased by more than 1° by post-depositional compaction (Helland-Hansen, 1992, Plink-Björklund, 2002). Their amplitudes are typically reported to be in the range of 100–250 m (Helland-Hansen, 1992; Johannessen & Steel, 2005), or more rarely up to 350 m (Plink-Björklund et al., 2001).

The clinothems of the Battfjellet Formation consist of shelf to slope and basin-floor deposits (Helland-Hansen, 1990; Steel & Olsen, 2002; Mellere et al., 2002). Sand-prone sediments were trapped on the shelf-edge and upper slope, forming basinward-thinning wedges, or on the shelf as stacked shoreface to deltaic parasequences. (Plink-Björklund et al., 2001; Johannessen & Steel, 2005; Grundvåg et al., 2014a). However, some clinothems show evidence of sand transport to the basin floor (Plink-Björklund et al., 2001; Steel & Olsen, 2002; Crabaugh & Steel, 2004; Johannessen & Steel, 2005). Clinothem 12 is one such clinothem and is the focus of this study. The study area is part of the renowned Van Keulenfjorden transect at the southwestern flanks of Storvola and Hyrnestabben, where Clinothem 12 is interpreted to represent slope and basin floor fan deposits (Crabaugh and Steel, 2004; Clark & Steel, 2006). The coeval shelf-delta deposits occur further to the west on the neighbouring mountain of Brogniartfjella (Steel & Olsen, 2002; Johannessen & Steel, 2005).

Field Methods

Eight stratigraphic logs, totalling 140 m in thickness, were collected along a 4.7 km transect of the exposed basin-floor fan of Clinoform 12 (Fig. 1C). The logs record lithofacies, grain size (based on field observations), bed thickness, sedimentary structures, presence of organic matter (i.e. plant debris), bounding surfaces, and palaeocurrents from flute marks and current ripples. The stratigraphic logs comprise the exposed vertical succession of the sand-prone basin-floor fan at the outcrop locations. The heterolithic lower part of the fan is commonly weathered and covered by scree. Logs were correlated by assigning depositional sub-environments based on their lithofacies association and bounding surfaces (Prélat et al., 2009). Sandstone samples were collected every 1–2 m near the base of the sampled beds (at about 2–3 cm from the base) to avoid biasing towards specific bed divisions or sedimentary structures. Sampling just above the bases of beds may under- or overestimate the grain size of the entire bed as massive turbiditic sands can show inverse grading, normal grading, or a lack of grading (Sylvester and Lowe, 2004). However, most often the bed bases give a good representation of the more energetic part of the flow and the consistency is needed to compare lobe sub-environments over longer distances. Within the investigated succession, one lobe with a complete proximal to distal preservation could be recognized and only those samples (66) that are located within that lobe were selected for evaluation of the longitudinal grain size distribution (Figs. 2 and 3).

Depositional architecture of the basin floor fan

Thickness, lithofacies and palaeoflow directions

Clinothem 12 is formed by two sand-prone intervals that are separated by a thin-bedded heterolithic package and silt-prone package. Both sand-prone packages have an approximately 15 m maximum thickness. The separating heterolithic/siltstone-prone interval has a maximum thickness of 4.5 m. The maximum exposed total thickness of 33 m is measured in log 7 (Fig. 2). Poor exposure up-dip of Log 7 prevents assessment of the total thickness in logs 2–6. In addition, the lowermost, heterolithic part of the sections are commonly scree covered, hindering accurate thickness measurements of the distal lobe fringe facies. A thinning of the clinothem can be observed distally of Log 7. The total thickness of the deposits thin from approximately 33 m (log 7) to 13 m at Hyrnestabben (estimated thinning rate of 11 m/km). In the intermediate part of the studied section a 4 m thick folded heterolithic sandstone unit can be observed on the base of the upper sand package. A detachment zone to its base suggests that part of the underlying succession may have been eroded as the deposits were remobilised.

A limited set of palaeoflow directions (n=26) measured from flute marks and current ripples of Clinothem 12 deposits resulted in two different directions: 195 and 118 degrees, respectively. Flute marks account for the southern palaeoflow indicators, while palaeoflow measurements taken from ripple laminations point to the southeast. Crabaugh and Steel (2004) reported east to southeast directed flute casts for Clinoform 12.

A bimodal flow direction in confined basins is likely caused by deflection and reflection of flow from side slopes and topographic highs (Spotts, 1964; Kneller et al., 1991; Haughton, 1994; Kneller and McCaffrey, 1999; Pohl and McCann, 2014). Crabaugh and Steel (2004) suggested flow diversion within the basin-floor fan of Clinoform 14 which changed from basinward to slope parallel at the most distal part and proposed that tectonically-induced topography influenced fan deposition. They propose that the basin-floor fan of Clinothem 12 is not affected by such tectonic activity during sedimentation. However, influence of confinement on flow directions cannot be entirely discarded.

The main palaeoflow direction assumed from the measurements in this study is to the southeast and conforms to basinward growth of Clinothem 12 towards the southeast reported by Crabaugh and Steel (2004). We would like to mention though, that the positioning of individual lobes forming the basin-floor fan is likely more variable.

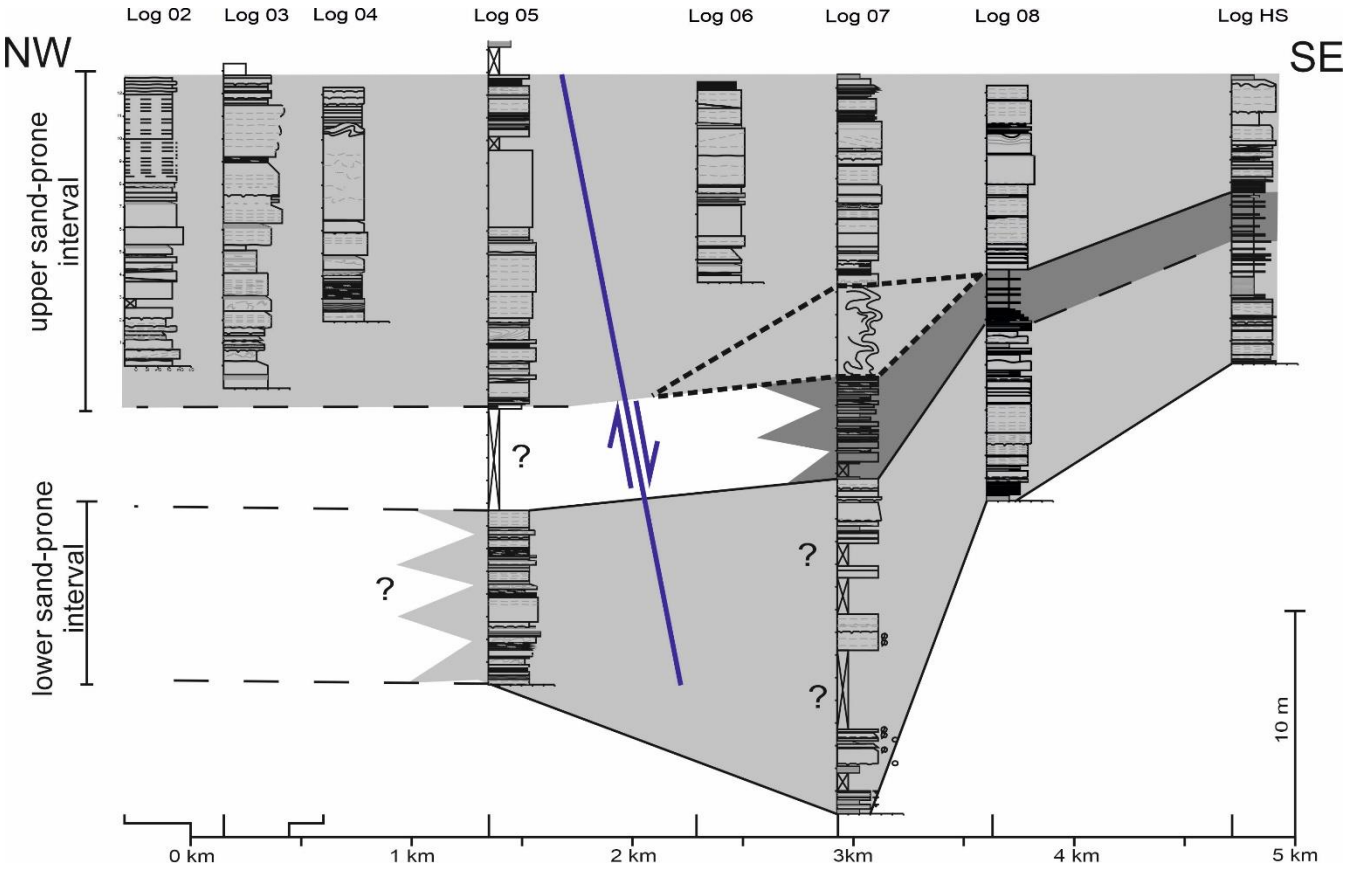

Fig. 2: Correlation panel of Clinothem 12. Uncertain correlations are pointed out with dashed black lines. Red lines indicate erosion surfaces. The normal fault between log 5 and log 6 is marked by a dark blue line. The slumped unit of the upper lobe/lobe 2 is marked by a stippled black polygon. The indicated fault between Log 5 and Log 6 is interpreted as post-depositional and serves orientation purposes only.

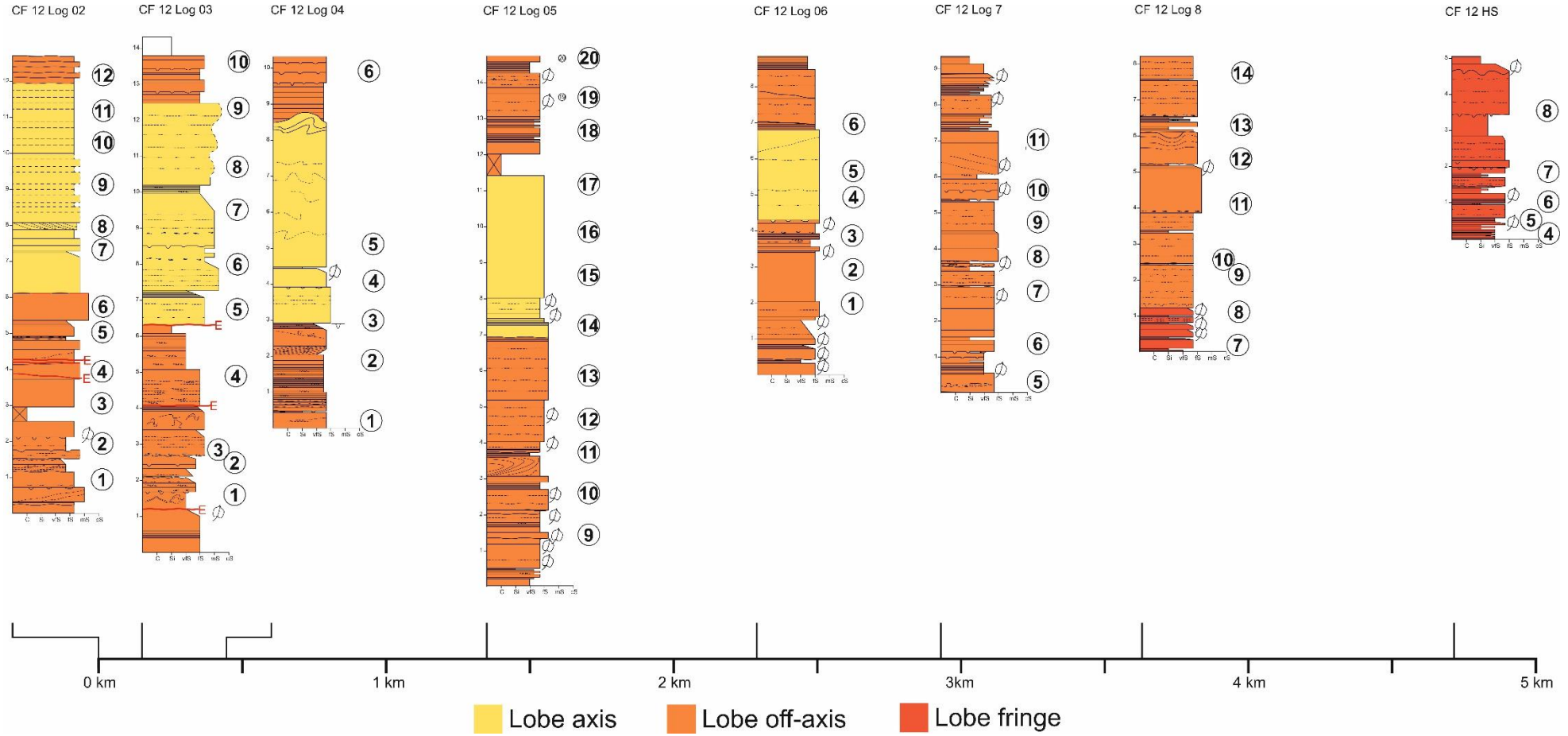
CF 12 Log 02
CF 12 Log 03
CF 12 Log 04
CF 12 Log 05
CF 12 Log 06
CF 12 Log 7
CF 12 Log 8
CF 12 HS
0 km
1 km
2 km
3km
4 km
5 km
Lobe axis
Lobe off-axis
Lobe fringe

Fig. 3: Locations of samples and sample number taken within the deposits of the youngest lobe. Colours indicate the interpreted lobe sub-environment from field data alone.

Lithofacies

Lithofacies encountered in the outcrop (Fig. 4) are summarized in Table 1**.** Four depositional sub-environments were interpreted based on characteristic lithofacies associations: lobe axis, lobe off-axis, lobe fringe, and lobe distal fringe (*sensu* Prélat et al., Etienne et al. 2012; Prélat and Hodgson, 2013; Grundvåg et al. 2014b; Spychala et al. 2015; Marchand et al. 2015; Masalimova et al. 2016; Spychala et al., 2017a) (Fig. 5).

Lobe axis. Lobe axis deposits are comprised of thick-bedded (0.75 to 1.2 m) structureless sandstone (F1, Fig. 4B), thin- to medium bedded (0. 1 to 0.4 m) highly amalgamated sandstone (F1), planar laminated and stepped laminated sandstone (F2, Fig. 4C). The lobe axis association is characterised by > 95 % sandstone. Bed bases locally cut down up to 15 cm into underlying beds. Siltstones (F6, Fig. 4E) are rarely observed. Amalgamation is very common and results in sandstone packages to up to 3.4 m thick. Deposits of the lobe axis are mostly tabular, but can also show low-relief pinching and swelling due to minor compensational stacking of beds.

Lobe off-axis. Lobe off-axis deposits are dominated by planar laminated sandstone (F2, Fig. 4C), structured sandstone (F3, Fig. 4D) and subordinated structureless sandstone (F1, Fig. 4B). Siltstone deposits (F6, Fig. 4E) separating individual sand beds are more common than in the lobe axis. This facies association is characterised by 82–100% sandstone. Deposits are mostly thin- to medium bedded (0.1 to 0.5 m), but occasionally thicker beds are present. Beds are tabular and can be traced for several tens of metres across the extent of the studied outcrop segments.

Lobe fringe. Lobe fringe deposits comprise planar laminated sandstone (F2, Fig. 4C), structured sandstone (F3, Fig. 4D), heterolithic packages (F4, Fig. Fig. 4E), hybrid beds (F5, Fig. 4G) and siltstone (F6, Fig. 4E). From all the facies association the lobe fringe facies association is the most variable in facies and bed thicknesses, which range from thin-bedded to thick-bedded (0,05 to 1.1 m). Lobe fringe deposits are characterised by < 70% sandstone. The transition of lobe fringe to distal lobe fringe is marked trough the change from variable thickness packages to thin-bedded intervals with very low sand percentages (< 20%).

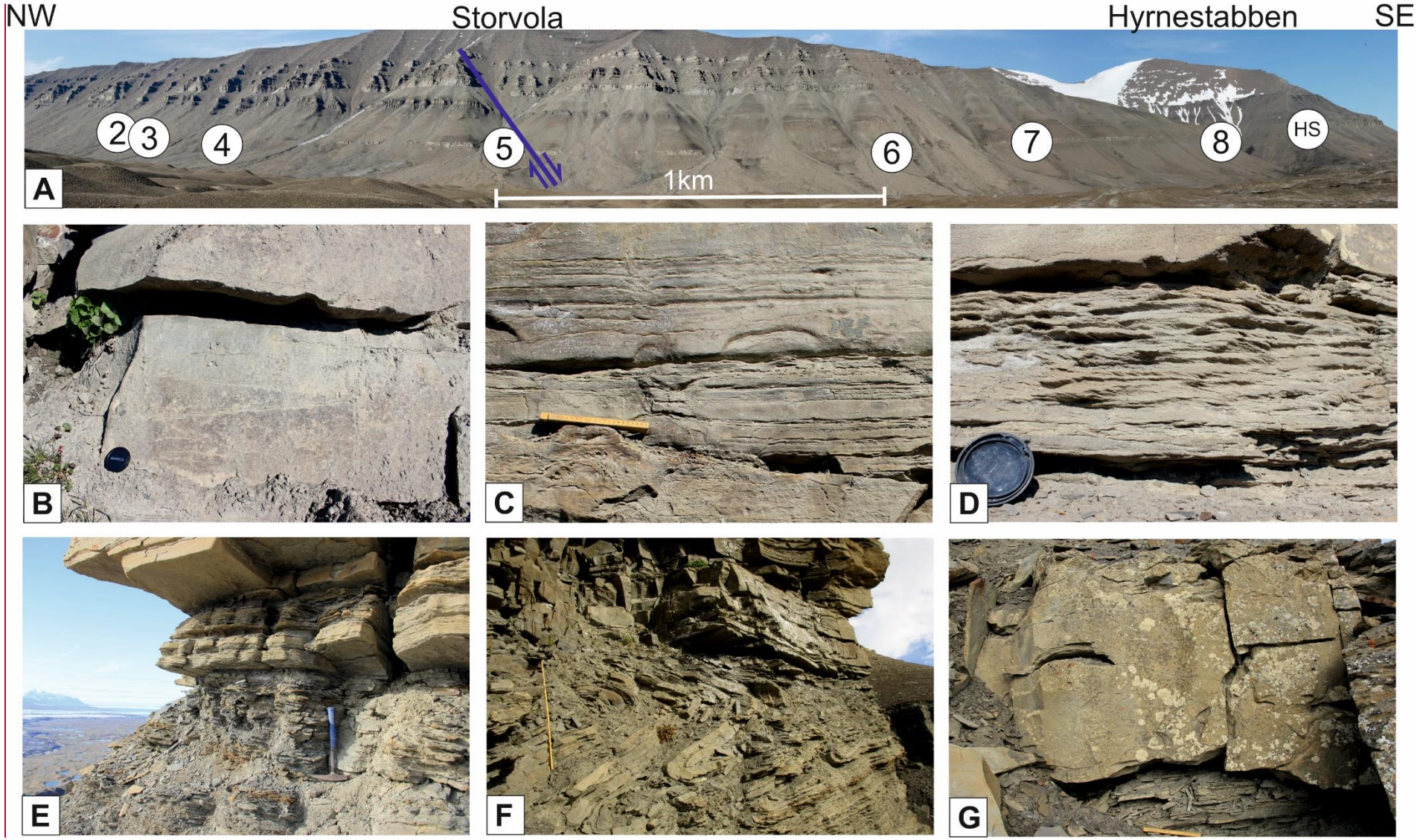
NW
Storvola
Hyrnestabben
SE
2
3
4
5
6
7
8
HS
1km
A
B
C
D
E
F
G

Fig. 4: A) Photopanel of the study area with Storvola in the foreground and Hyrnestabben in the background to the right. Log locations are indicated with their numbers. Indicated normal fault is post-depositional and for orientation purposes only. B) Example of F1: structureless sandstone. Lens cover as scale (~ 7 cm diameter). C) Example of F2: planar laminated sandstone. Folded rule (20 cm) as scale. D) Example of F3: Structured sandstone. Here the deposit shows ripple laminations. Lens cover as scale (~ 7 cm diameter). E) The log section at Hyrnestabben (Log HS) shows F6 (siltstones) at its base which are overlain by F4 (heterolithic interval). Geological hammer (30 cm) as scale. F) Folded sandstones at the base of the youngest lobe in the section of Log 7. Rule (100 cm) as scale. G) Hybrid bed (F5) at Log HS. Note the irregular transition from clean sandstone to the debritic division which is weathered back into the slope. Folded rule (20 cm) as scale

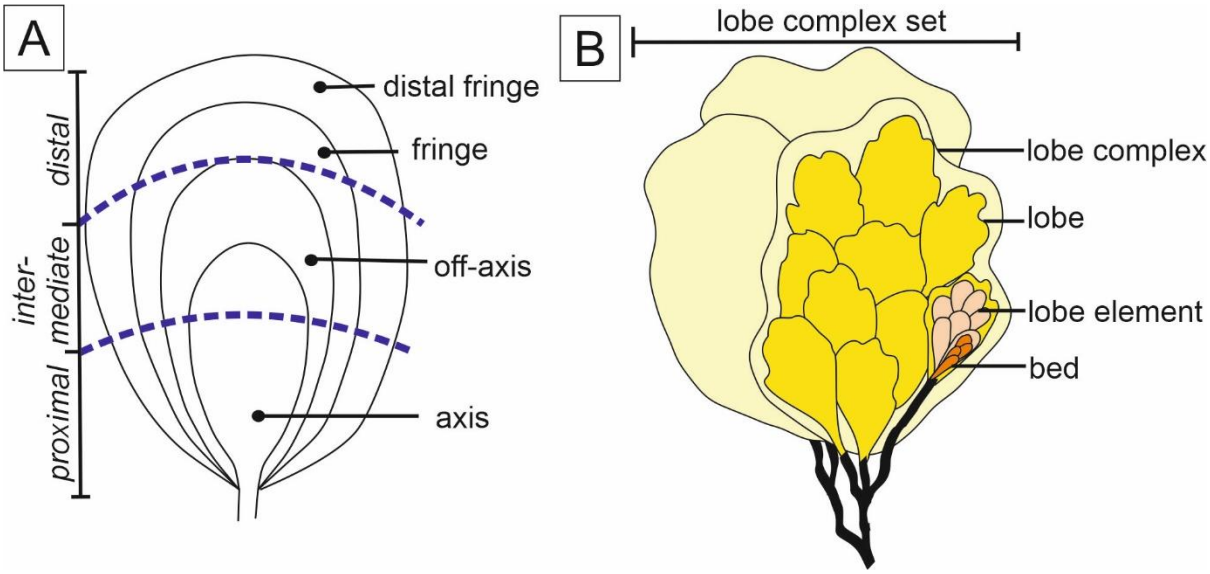

Fig. 5 A) Simplified model indicating the various sub-environments in a lobe (redrawn from Prélat et al. 2009). Stippled blue-lines indicate proximal, intermediate and distal lobe areas. B) Plan-form view of five-fold lobe hierarchy: bed to bed set, lobe element, lobe, lobe complex, and lobe complex set (modified from Prélat et al. 2010, redrawn from Spychala et al., 2017a).

Distal lobe fringe. Distal lobe fringe deposits are dominated by structureless and planar laminated siltstones (F6, Fig. 4E). Thin-bedded very fine sandstone beds can be observed to be intercalated within the silt-prone intervals. Distal lobe fringe deposit can form intervals up to 4.5 m thick.

Proximal and distal lobes

The terms ‘proximal’, ‘intermediate’ and ‘distal’ lobe are descriptive and reference to spatial areas of the deposits rather than indicating a sub-environment. It has to be noted these terms are not officially defined and are therefore not used consistently by different authors. Figure 5A shows the definition of these terms for our study. The proximal lobe is located up-dip, close to the feeder channel and is dominated by lobe axis deposits, but can also

encompass lobe off-axis and lobe fringe deposits laterally. The intermediate lobe comprises dominantly lobe-off axis deposits, but may also comprise deposits from all other lobe sub-environments. Geographically the intermediate lobe is neither close to the feeder channel nor to the lobe pinch-out. Finally, the distal lobe is characterised by deposits from the lobe fringe and lobe distal fringe only. It is located down-dip and marked by its association with the down-dip pinch-out of the sandy lobe deposits.

Hierarchy of Clinothem 12

Lobe deposits commonly exhibit a five-fold hierarchy (e.g. Deptuck, 2008, Prélat et al., 2009, Grundvåg et al., 2014b, Spychala et al., 2017a): 1) a 'bed' represents a single depositional event; 2) one or more beds stack to form a 'lobe element'; 3) several lobe elements that are divided by thin siltstone intervals form a 'lobe'; 4) one or more genetically related lobes stack to form a 'lobe complex'; and 5) one or more lobe complexes within the same lowstand systems track stack to form lobe complex-sets (Fig. 5B).The studied section of Clinothem 12 conforms to the hierarchical level of lobe complex. The lower and upper sandstone-prone intervals conform to two lobes which are separated by lobe fringe deposits (thin-bedded heterolithic package), suggesting that there were genetically related sandstone-prone lobe deposits lateral to the exposed study area. Occurrence of hybrid beds in the most distal logged section at Hyrnestabben (Log HS; Fig. 1C) points toward the youngest lobe being exposed in a near dip-section as frontal lobes are more likely to exhibit hybrid bed deposits (Spychala et al., 2017 a,b). However, it cannot be excluded that the exposure may be slightly oblique to the main palaeocurrent direction.

Grain-size evaluation

Procedure

Thin sections with a thickness of 30 μm were produced from 66 samples, and these thin sections were photographed with a high-resolution camera under a Leica microscope. Samples were counted by grid counting manually outlined grains using image processing software (ImageJ) which automatically records the long- and short-axis and orientation of the long-axis based on the best fitting ellipse of the grains. The grid size was kept at 0.03 mm^2. Per sample 300 grains were measured to provide sufficient accuracy even for very poorly sorted sandstones (Johnson, 1994).

Table 1 Observed lithofacies in Clinothem 12, their processes and depositional environment.

Lithofacies	Grain size	Thickness range	Description	Process interpretation	Depositional environment
Structureless sandstone (F1)	fs to ms	0.25 - 1 m	Ungraded to graded; top can show 1) a silty cap, and/or 3) coal fragments (occurrence increases from CF12-3 to CF12-7); bases are sharp or loaded; often groove and flute casts on base; outsized clasts of up to 3 mm; dewatering structures; mudclasts (1-2 cm) at discrete horizons; up to 3.4 m in highly amalgamated intervals; 10-15 cm of erosion can occur at the base	Deposited by high-density turbidity currents (Kneller and Branney 1995) with high aggradation rates (Arnott and Hand 1989; Leclair and Arnott 2005; Talling et al. 2012a)	lobe axis
Planar laminated sandstone (F2)	fs to ms	0.25-0.5 m	Planar laminated are either flat or slightly inclined; Planar laminations can be at the top of F1 beds or throughout the bed; Stepped planar laminations are observed from the base of beds	Deposited by high-density turbidity currents. Planar laminations are produced by reworking of the bed (Allen 1982; Southard 1991; Best and Bridge, 1992), Stepped planar laminations are produced by rapid sediment fallout (Hiscott	lobe axis or lobe off-axis
Structured sandstone (F3)	vfs to fs	0.05- 0.25 m	wavy to sinusoidal lamination; ripple cross-lamination; isolated ripples; climbing-ripple lamination; stratified laminations; flame structures; horizontal bioturbation; bed bases and tops are commonly sharp and flat	Deposited by low-density turbidity currents. Wavy or sinusoidal lamination indicates deposition from waning currents with very high rates of suspension fallout (Allen 1973; Jopling and Walker 1968; Hunter 1977). Current-ripple lamination produced by reworking through dilute flows along the bed (Allen 1982; Southard 1991; Best and Bridge 1992). Climbing ripple lamination forms under bedload transport associated with high aggradation rates (Allen 1973;Hunter 1977; Jobe et al.	lobe off-axis
Heterolithic package (F4)	silt and vfs	0.2- 0.5 m intervals	1) lenticular sandstone bodies in siltstone, 2) intercalated tabular vfs and siltstone, or 3) dominantly siltsone (70 to 90%) with minor sandy beds (2-5 cm thick); sandstone beds can show planar, ripple or wavy lamination	Deposits of distal, sluggish, low-volume flows (cf. Jobe at al. 2012). Ripple lamination form beneath dilute turbulent flows via reworking of the bed under moderate aggradation rates, whereas climbing-ripple lamination forms under high aggradation rates (Allen 1971; Allen 1982; Southard 1991)	lobe fringe
Hybrid beds (F5)	csilt to fs	0.15- 1.2 m	Lower sandstone division, usually structureless, rip-up clasts (up to 30 cm) on discrete horizons; upper muddier matrix with abundance of mudchips and coal fragments; poorly sorted; can be slightly graded at their tops	Co-genetic turbidity currents (lower division) and cohesive debris flows (upper divisions) (Haughton et al. 2003; Talling et al. 2004; Haughton et al. 2009; Hodgson 2009).	lobe fringe
Siltstone (F6)	fsilt to csilt	0.01-0.02 m	Planar bedded siltstone; mostly structureless; some beds show faint lamination	Deposited by dilute turbidity currents. Planar lamination is a product of traction (Stow and Piper 1984; Mutti 1992; Talling et al. 2012a). Structureless beds are formed by direct suspension fallout (Bouma 1962)	distal lobe fringe to background sedimentation
Folded sandstone (F7)	vfs to fs	0.55 to 4 m intervals	Folded and overturned beds of 5-15 cm thickness; some ripple laminated beds, but mostly structureless and normal graded; Bases of chaotic and folded units are sharp to erosive, while bed tops are sharp	Syn-depositional deformation due to remobilization of local thin-bedded stratigraphy. The low amount of disaggregation supports an interpretation of slump deposits	not indicative of a specific environment

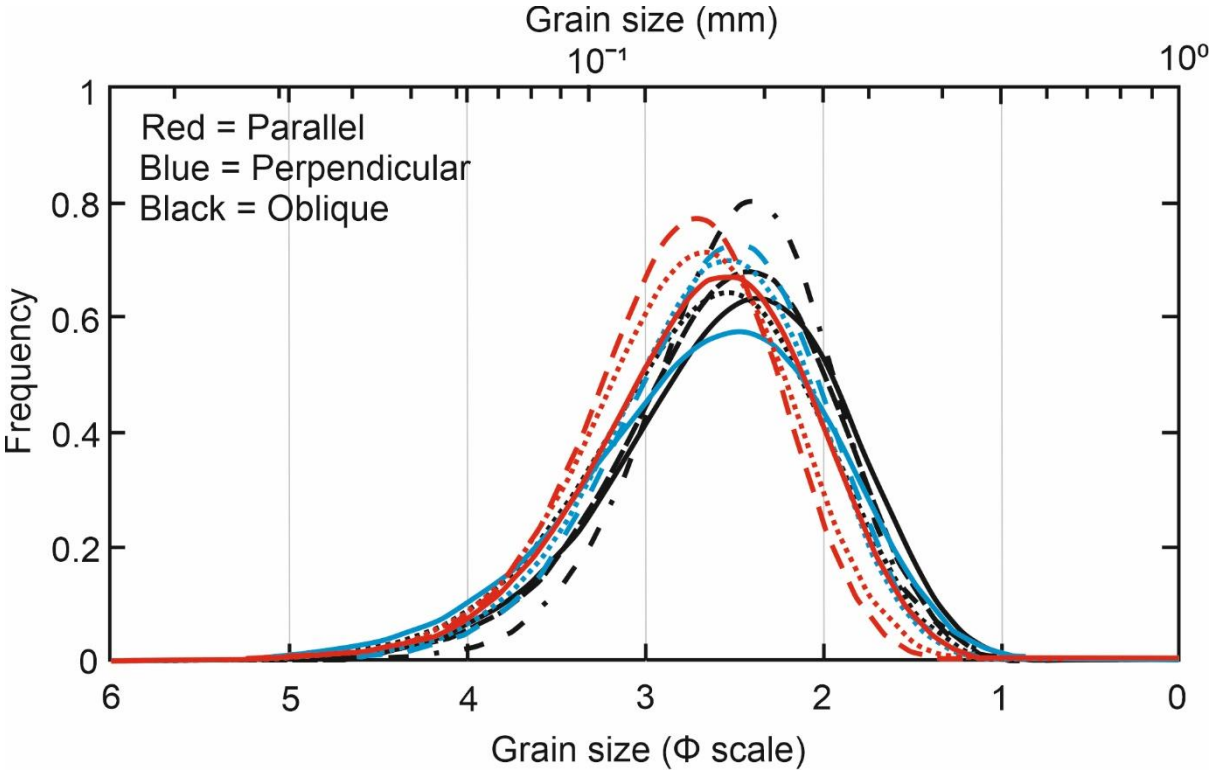

Fig. 6: Master sample grain size elevation: *Grain-size distributions of oriented samples with respect to the palaeoflow analyzed by three different operators. The line styles represent the operators.*

To correct for underestimation of the spherical-grain mean values due to cutting effects, the recorded long- and short-axis are multiplied by 1.1318 (Johnson, 1994). The true nominal grain diameter (the diameter of a sphere with the same volume as the considered particle) was calculated following Johnson (1994):

$$D'=d'+0.4(a'-d')2 \quad (1)$$

where D' is the true nominal diameter (mm), and d' = (a' b')1/2, and a' and b' are the corrected long- and short-axes (mm), respectively. True nominal grain diameters were converted to ϕ-scale (ϕ = -log2 (Dmm); Krumbein, 1934) to give the most satisfactory representation of the distribution (Johnson, 1994). Determining grain size from photographed thin sections causes a lower precision for grains below the thin-section thickness (Johnson, 1994; Sylvester and Lowe, 2004; de Leeuw, 2017) as they might overlap each other. A lower limit for grain size measurement was placed at 30 µm in this study. This limit excludes fine-silt from our grain-size measurements. The obtained grain-size distributions in ϕ are approximately normally distributed and suggest a log-normal distribution

on the metric scale. Descriptive statistical measures (mean (*M*), standard deviation (σ), skewness (*S*), and kurtosis (*K*)) are calculated using MATLAB.

To test the hypothesis that grain-size distributions of lobe sub-environments are statistically different an analysis of variance (ANOVA) was applied to the mean grain-size of the distributions. ANOVA compares the 'variance between/among' grouped data with the 'variance within' a group. For this study the grouping will be based on lobe sub-environments: lobe axis, lobe off-axis, and lobe fringe.

Measurement Errors

Two types of measurement error were investigated by dissecting a single sample in multiple orientations (orientation error) and counting grain sizes by multiple operators (operator error). The observed differences between groups of samples need to clearly exceed these measurement errors for the results to indicate significant differences.

Orientation error

Non-spherical grains are frequently arranged in specific patterns with respect to the palaeoflow direction (Hiscott and Middleton, 1980; Arnott and Hand, 1989; Baas et al., 2007). In turbidites, a flow-aligned fabric (with the long axis aligned with the palaeoflow direction) is favoured during relative rapid sedimentation from suspension, whereas flow-transverse fabric is the result of grain transportation along the bed by traction during relatively low sedimentation from suspension. Oblique fabric appears to be restricted to massive sandstone turbidites but the mechanism causing this fabric is still unclear (Baas et al., 2007).

For consistency, all selected samples (66) were cut perpendicular to the bedding with most samples (51) cut parallel to the assumed main palaeoflow direction of 118°. For some samples the orientation of the samples could not be reconstructed after returning from the field. And for other samples, the limited number of paleoflow measurements taken from few other beds, sometimes in another stratigraphic section, could be a poor reflection of the true transport direction of that sample. These uncertainties necessitate a careful assessment of the measurement errors related to the orientation of the thin sections relative to the palaeoflow orientation. For this purpose, one sample was selected and cut parallel, perpendicular, and oblique (45°) to the assumed main palaeoflow direction of 118°. The data show that the measured grain size indeed varies depending on the orientation of the thin section with respect to 118°, which illustrates the error of cutting the sample in different orientations (Fig. 6). The pooled standard deviation ('weighted average standard deviation') for different orientations of the sample is 0.06 ϕ.

Operator error

The three thin-sections of the sample were analysed by three different operators to test the effect of operator-choices in outlining individual grains. The pooled standard deviation ('weighted average standard deviation') for the error due to individual operator choices is 0.11 ϕ. Based on this analysis, the decision was made to evaluated all samples by a single operator (T.A.B. Ramaaker) to ensure consistent application of grain-delineations and avoid inter-operator errors.

Grain-size distribution

Figure 7 illustrates the grain-size distributions of 19 lobe axis samples, 40 lobe off-axis samples, and 7 lobe fringe samples. With the exception of a few grains, measured individual grain sizes range from 0 to 6 ϕ (1000 µm to 30 μm; coarse sand to medium silt). The grain-size distributions show mean grain-size values ranging from 2.06 to 4.03 ϕ *(*239 µm to 61 μm*)* with an average mean of 2.89 ϕ *(134* µm*)* (standard deviation of 0.33 ϕ). 56 of the 66 samples have a mean grain-size between 2.5 and 3.5 ϕ (177 µm to 88 µm) with only 1 sample being finer than 3.5 ϕ (4.03 ϕ). Modal grain size ranges from 1.57 to 3.95 ϕ (336 µm to 64 µm) and indicates an overall slightly skewed distribution towards finer material (excess of finer material).

Most samples are moderately well sorted (standard deviation of 0.5–0.7 ϕ) or moderately sorted (σ: 0.7–1.0 ϕ). Especially the lobe off-axis samples are predominantly moderately well sorted. Grain-size curves of the measured samples are mainly symmetrical (skewness of -0.1–0.1) but can be fine skewed (0.1–0.3) indicating a tail of finer grains.

Grain-size distribution within sub-environments

The lobe sub-environments have similar distribution curves within each group, but show significant differences between groups. Lobe axis (Fig. 8A), lobe off-axis (Fig. 7B), and lobe fringe (Fig. 8C +D) have mean grain-size values of 2.68 ϕ (156 µm; standard deviation (σ (ϕ)) of 0.20), 2.91 ϕ (133 µm; σ *(*ϕ*)*: 0.29), and 3.30 ϕ (101 µm; σ *(*ϕ*)*: 0.43), respectively. The Analysis of Variance (ANOVA) of the mean grain-sizes indicates that all three sub-environments are statistically different at a confidence level of 99%. Although the mean grain-size values are distinctly different, there is still overlap between the grain-size distribution curves which means no sub-environment has a discrete grain size range that separates them form the other sub-environments.

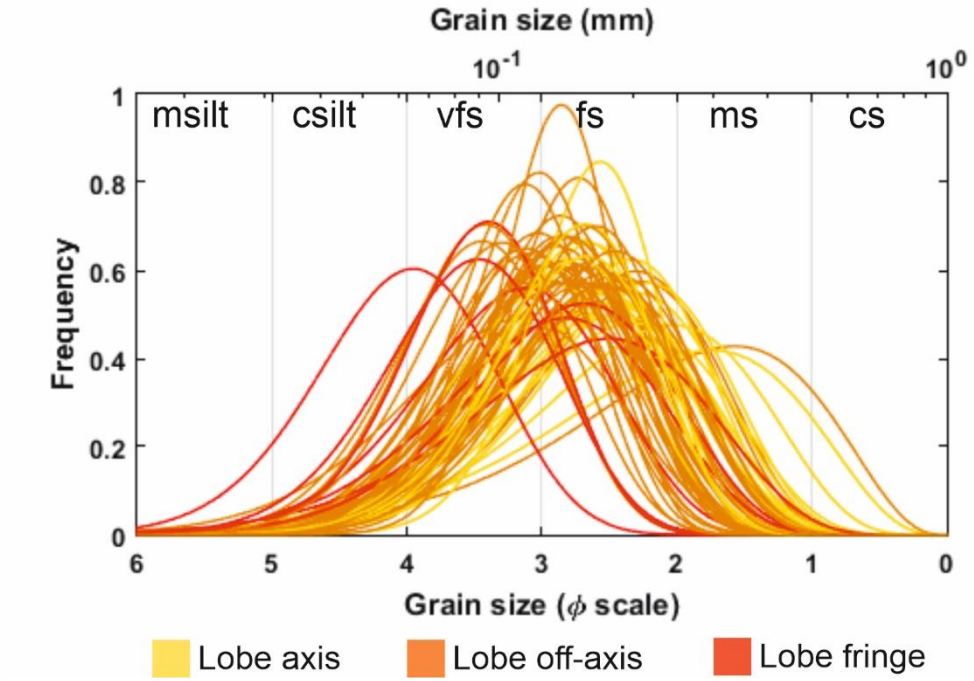

Fig.7: Probability density functions of the grain-size distributions of basin-floor fan deposits of Clinothem 12 showing all 66 grain-size distributions of lobe axis (yellow), off-axis (orange), and fringe (red) samples.

Lobe axis, lobe off-axis as well as lobe fringe have samples that are fine skewed (Fig. 9). No relation between mean grain-size and bed thickness (of sampled beds), standard deviation, skewness, or kurtosis could be observed to be characteristic for any sub-environment.

Lobe sub-environments were defined based on lithofacies implying a possible difference in grain orientation between lithofacies associations which could affect the grain-size distribution. However, the observed difference in grain-size distribution between the different cutting orientations (0.06 ϕ) is significantly smaller than the difference between lithofacies associations. Furthermore, the range within the sub-environments is significantly larger than the deviation caused by cutting orientation, which indicates that true variability is larger than measurement error both within sub-environments and between sub-environments.

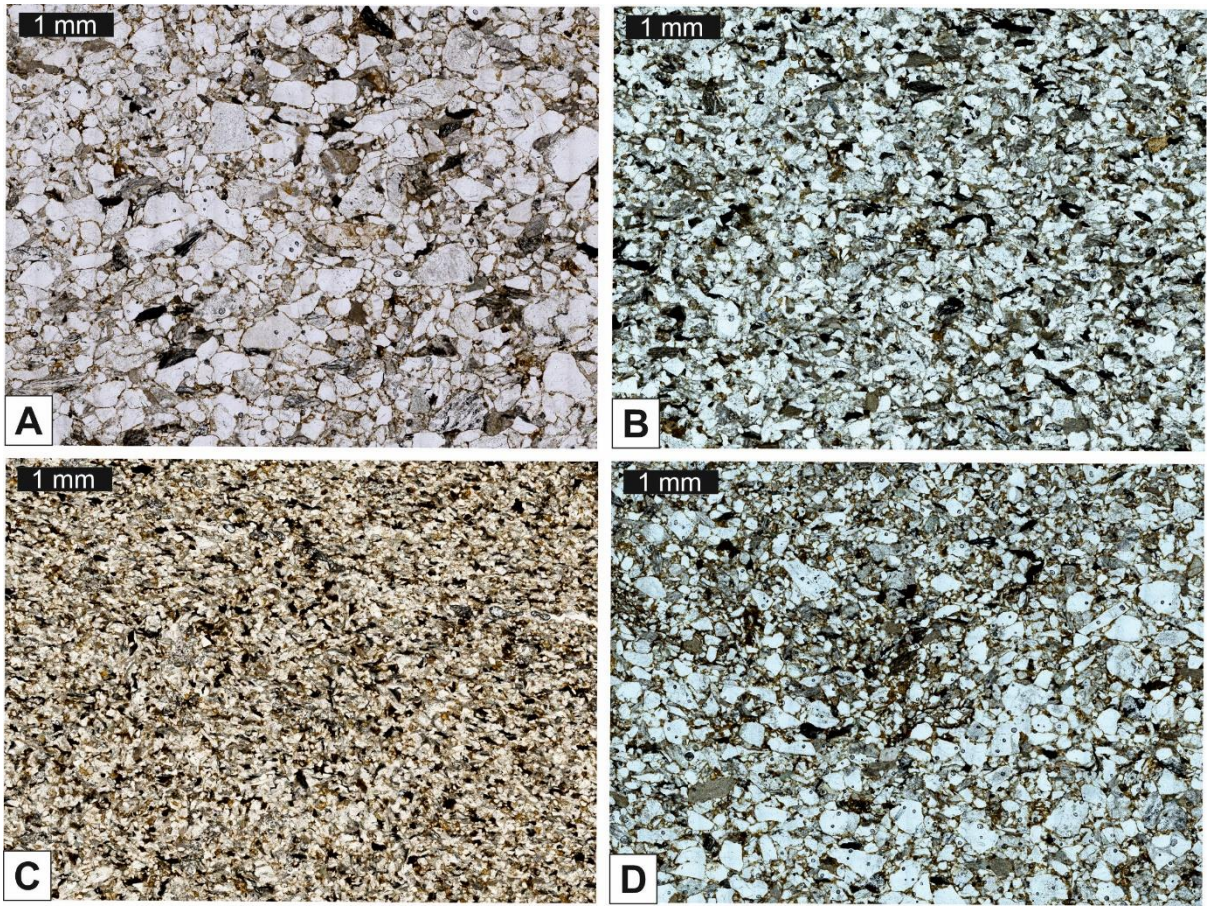

Fig.8: Examples of lobe sub-environment lithology and grain size in thin-sections. A) Lobe axis. Sample 6 of Log 3. B) Lobe off-axis. Sample 12 of Log 5. C) Lobe fringe. Sample 4 of Log Hs. D) Lobe fringe hybrid bed. Sample 8 of Log HS.

Longitudinal trends

A regression analyses of the mean grain-size of all samples shows a moderate negative correlation (R = - 0.51) with distance over 5 km (Fig. 9). However, samples with mean grain sizes coarser than 2.5 ϕ (177 µm) are only observed in the most proximal part of the basin-floor fan. Samples with mean grain size between 2.5 and 3.5 ϕ (177 µm to 88 µm) can be observed throughout the dip-section without a clear decrease in value. The finest mean grain sizes are recorded in the distal fringes of the Hyrnestabben section. Looking at longitudinal grain-size distributions of the interpreted lobe sub-environments separately a more detailed pattern can be seen. Lobe axis settings reach halfway of the exposed lobe section and show a relatively stronger correlation with distance (R= - 0.56; Fig. 10). Lobe off-axis deposits occur along the entire studied transect (more than 3.5 km) with the exception of the most distal log at Hyrnestabben (Fig.1C). Samples from these off-axis deposits only show a weak decrease in mean grain-size (R= -0.23). For these samples no correlation between distance and

any other parameter is found. Lobe fringe deposits collected from Log 8 and HS (Fig. 2) indicate a decrease in grain size (R= -0.42; Fig. 10) over a distance of roughly 1 km.

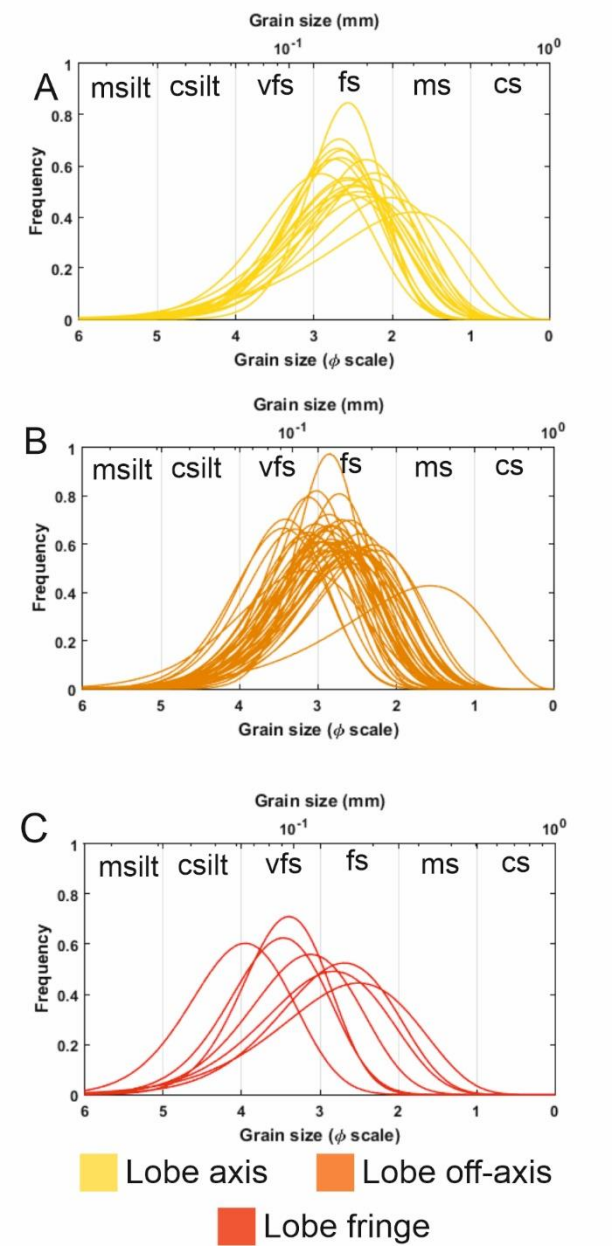

Fig. 9: Probability density functions of the grain-size distributions of lobe sub-environment deposits of Clinothem 12. A) Lobe axis. B) Lobe off-axis. C) Lobe fringe.

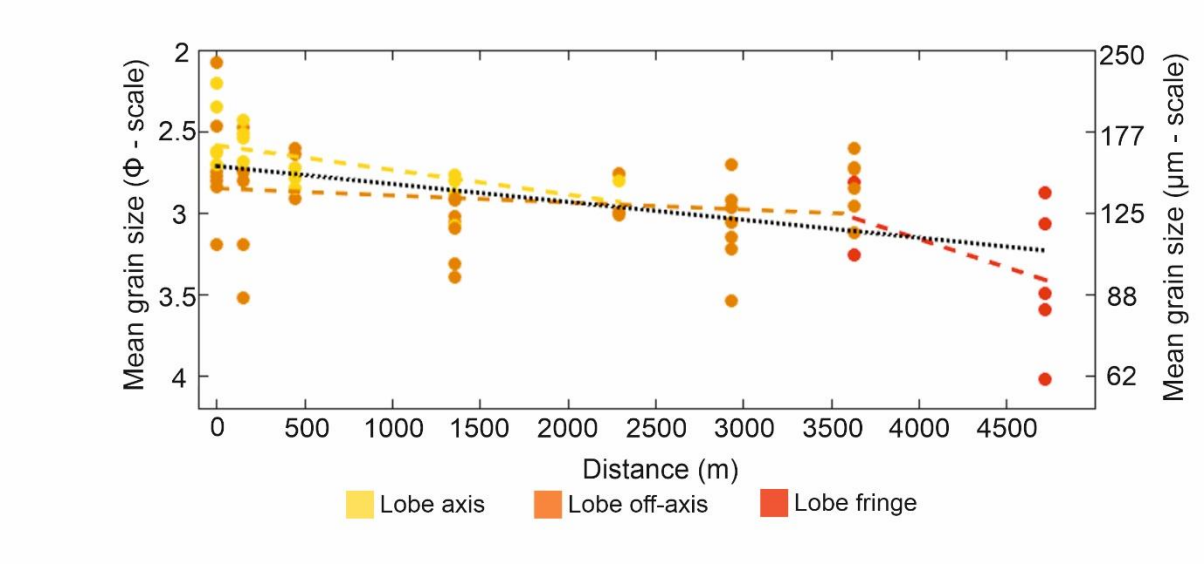

Fig. 10: Longitudinal development of mean grain-size. Black dotted line indicates the linear regression of the mean grain-size of all samples with longitudinal distance (R=-0.51). Lobe axis, off-axis and fringe samples and their linear regression with distance (R= -0.56, R= -0.23, and R= -0.42, respectively) are indicates by the yellow, orange, and red points and dotted lines, respectively. Note the relative stable range in mean grain-size of lobe off-axis samples.

Vertical trends

Vertical trends through the individual logs are illustrated in Figure 11. No absolute datum is present throughout the section to retrieve absolute vertical positions within the lobes, and each log has a different thickness. Therefore, a relative elevation is defined reaching from 0 (lower boundary of the lobe) to 1 (upper boundary of the lobe) in each log.

No obvious overall vertical coarsening or fining trend is observed (Fig. 11). Only the most distal location (Log HS) that consists solely of lobe fringe deposits has a vertical coarsening trend with mean grain-size shifting from 4.03 to 3.06 *ϕ (30 µm to 119 µm)*. Other logs appear to show a subtle coarsening to fining trend with the coarsest samples at the middle to upper part of the log. This is clearly observed in Log 2 where the lower 6 samples represent lobe off-axis and show a coarsening trend followed by 5 lobe axis samples that show an overall fining upwards. The lowermost samples of the logs are commonly relatively coarse. But these subtleties could be coincidence.

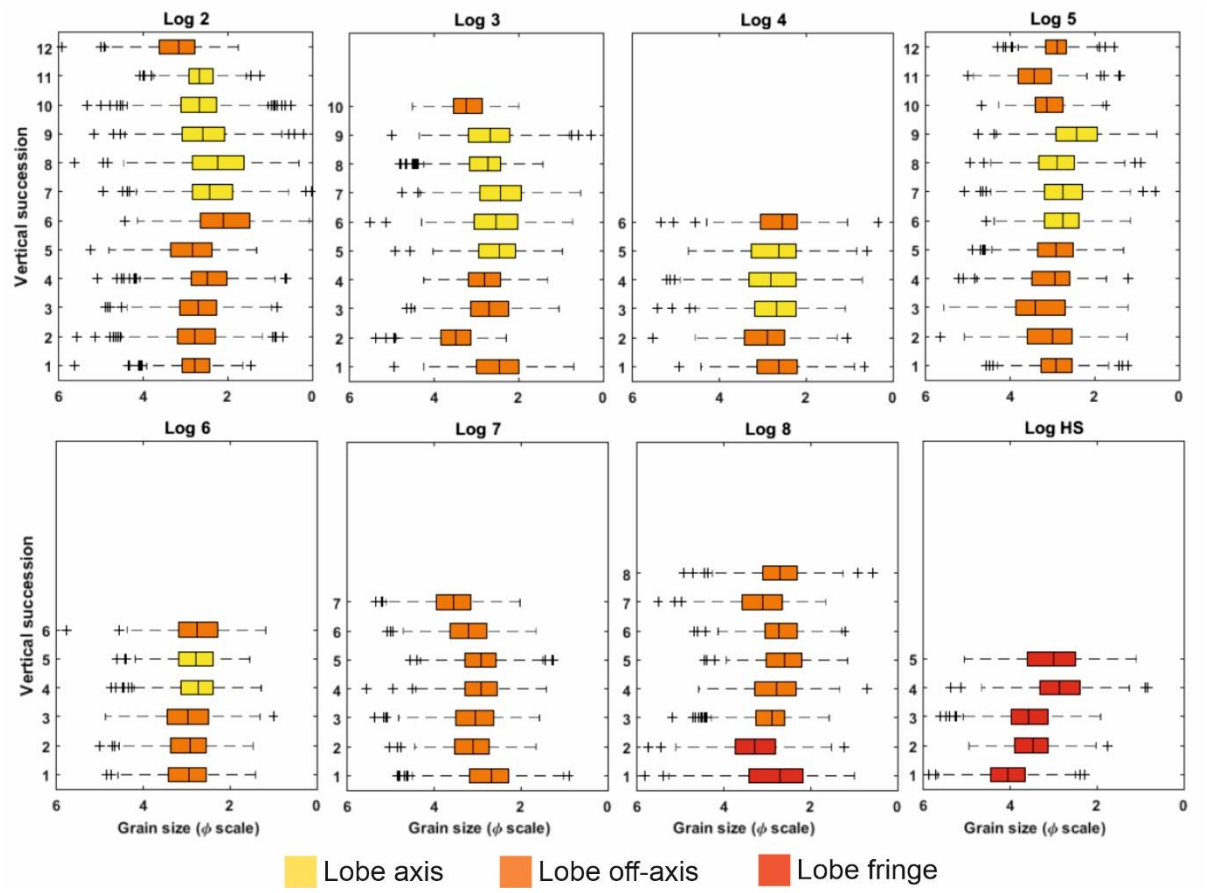

Fig.11: Boxplots of grain-size distributions in vertical succession (with 1 referring to the lowermost sample up to highest sample within the log) of individual logs. Colours indicate the sub-environments lobe axis (yellow), off-axis (orange), and fringe (red). The vertical line within the box indicates the median and the boundaries of the box indicate the 25th and 75th percentile. The whiskers, marked as ⊢ - -, extend 1.5 times the interquartile distance (distance between indicate the 25th and 75th percentile). The plotted whiskers extend up to adjacent value that is the most extreme data point within the calculated whisker. The outlier, marked as +, are values above or below the whiskers.

Discussion

Clark and Steel (2006) showed that basin-floor fans of the Battfjellet Formation consist mainly (75%) of fine sand (125–250 µm; 3–2 ϕ). Overall, this agrees with the grain-size distributions reported here, especially when considering Clark and Steel (2006) used the coarsest part of the beds to determine the grain size of the deposits. However, visual observations made in the field can neither record the range of grain sizes of individual deposits, which generates a sampling bias towards coarser grain sizes overall, nor the subtler differences in grain-size distribution between lobe sub-environments. The fact that almost all of our samples are slightly skewed towards finer material conforms to the observations Fildani et al. (2018) have reported from the lobes of the Mississippi Fan, that visual descriptions alone tend to overestimate the sand fraction of deposits. These considerations should motivate the research community to increase the integration of microscopic sample analyses into outcrop studies.

Grainsize distribution and sub-environments

The measured grain-size distributions of the lobe axis, lobe off-axis, and lobe fringe are significantly different suggesting that these sub-environments have distinctly different grain-size distributions (Fig. 12). Despite the fact that classifications of these sub-environments, based on macroscopic facies characteristics, are transitional, assigning lobe sub-environments to lithofacies associations proved to be a rather powerful method to differentiate the grain-size distributions within the scale of a lobe. Only one sample from the lobe off-axis group strongly differs from the other off-axis samples and is also the coarsest of all the samples. This sample, sample 6 of Log 2, was not classified during the macroscopic facies analysis as lobe axis, like the overlying deposits, because an erosional surface above the bed was chosen as lower boundary of the lobe axis at Log 2. Based on the grain-size distribution this sample could also be classified as part of the overlying lobe axis. Re-assigning individual samples to other sub-environments based on their microscopic grainsize distribution could be justified in practice, but would here generate the appearance of circularity: grainsize correlates with facies association, outlying grain size distributions are re-assigned to another facies association, and therefore also correlate to facies association. Therefore, no such re-interpretations based on the grain size results were made here to illustrate the power of the *a priori* distinction between sub-environments based on macroscopic facies characteristics.

As discussed in the section about grain size evaluation methods, the difference in grain size is not related to difference in grain fabric since the deviation due to orientation is much smaller than the deviation between and within the sub-environments. We assume that the grain fabric maturity of all samples is similar to the tested sample, implying that the obtained magnitude of difference in grain size with orientation is similar in all samples. This assumption might be invalid as the tested sample is retrieved from a massive turbiditic sandstone. This type of deposit features a broad range of long-axis orientations and possibly results in less variation with orientation compared to structured beds with more mature fabric (Baas et al., 2007). This possible larger difference in orientation is largely eliminated by sampling at the base of the beds, which mostly consist of massive sandstones.

Proximal to distal trend

The results that are presented in this study strengthen the idea that lobes do not just simply fine from an apex, but show a more complicated non-linear fining trend (Fig. 12). Lobe axis and fringe settings show a (weak) basinward fining trend, whereas lobe off-axis settings show no longitudinal

decrease in grain size (Fig. 12). The following section will discuss possible explanations for the observed fining trends:

Generally, there are two fundamental processes that govern deposition from a flow: competence and capacity. The competence of turbidity currents decreases from proximal to distal settings due to the loss in shear velocity, which is directly related to a loss of velocity (Kneller and McCaffrey, 2003; Kane et al., 2017). This decrease in flow velocity from the lobe apex is caused by the lateral spreading of flow, reduced sediment content due to sedimentation, and/or decreasing slope (Kneller, 1995), and is influenced by the topography of the lobe (Groenenberg et al., 2010; Spychala et al., 2017a). Sediment capacity describes the total amount of sediment a flow is able to transport. If a flow surpasses its capacity deposition is triggered by settling of the excess suspended sediment from the flow (Hiscott, 1994). It is argued that flows that exit the channel mouth are at or near their capacity limit when lobe deposition starts.

One explanation for the decrease of the grain-size profile in the lobe axis combines grain-size stratification with the transition into lower momentum flows that is associated with the channel-lobe transition zone (Baas et al., 2004; Fildani et al., 2018). As the flow velocity decreases capacity-driven sedimentation is invoked (*sensu* Hiscott, 1994; Kneller & McCaffrey, 2003; Kubo, 2004). The coarse sediment fraction tends to be concentrated near the base of turbidity currents, whereas the medium and finer sediment fraction are more homogenously distributed over the height of the current (Fig. 13; Garcia 1994; Kneller and Buckee, 2000; Hansen et al., 2015; Tilston et al., 2015; de Leeuw et al., 2018b; Eggenhuisen et al., 2020). This trend may be additionally promoted by the grain-size stratifications of flows (Fig. 13). Once the base (enriched in coarser grains) of the concentration profile has settled out, the off-axis is deposited from a flow with a relatively homogenous vertical grains size (Fig. 13). Eventually, the flow thins and decreases in density due to continued loss of sediment resulting in the onset of competence-driven deposition in the lobe fringes (Kneller and McCaffrey; 2003) creating a second fining trend. This likely goes hand in hand with the deposition of most of the remaining sand grains, creating the sand pinch-out described from field observations of the lobe fringe (e.g. Prélat et al., 2009, Spychala et al., 2017a) long before the silt pinch-out in the distal fringe (Spychala et al., 2020). This evolution of the flow as it deposits sediment on its journey across a lobe would overall result in fining from the lobe axis to the intermediate and distal areas of the lobe off-axis and lobe fringe, which conforms to the trend seen in the deposits of Clinothem 12.

Grain-size stratification has previously been widely used to explain grain size trends in submarine channel and canyon systems (e.g. Hiscott et al., 1997; Pirmez and Imran, 2003; Hubbard et al., 2014;

Hansen et al., 2015, Jobe et al., 2017; de Leeuw et al 2018a,b), but was sofar not taken into consideration as an explanation of fining trends in lobe deposits. Our study suggests that proximal to distal fining of lobe deposits is essentially the result of grain-size stratification in the flow exciting the channel, and the advection length of the different grainsizes (Ganti et al, 2014; Boulesteix et al., 2019, Spychala et al., 2020). These two processes therefor seem to be a viable starting point for simplified modelling approaches of lobe deposits. The Clinothem 12 lobe deposits documented in this study may serve as a testing ground for such models (please refer to supplemental materials for this studies Matlab file).

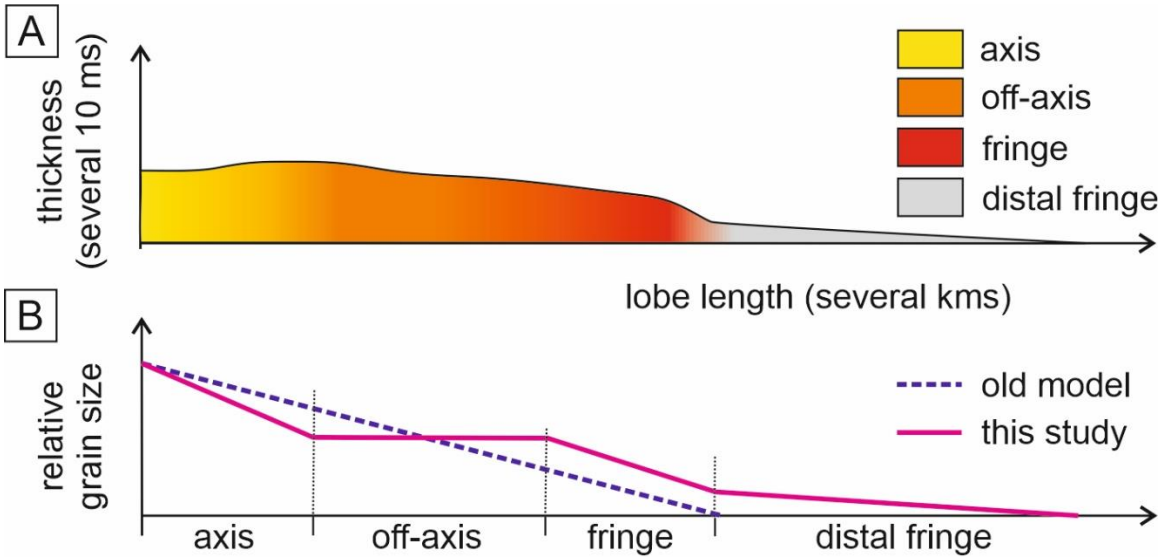

Fig. 12: A) Geometry and general distribution of lobe sub-environments. B) Longitudinal grain size evolution of lobe deposits. The old linear model is indicated in a blue dashed line, whereas the non-linear trend suggested by this study is indicated by a pink solid line.

Explaining the spread in lobe fringe samples

Lobe fringe samples collected from Log HS (Hyrnestabben, Fig. 1C +2) show a wide spread in mean grain sizes ranging from silt to fine sand (4.03 ϕ to 2.75 ϕ). It is noteworthy that the samples at this location were collected from lithofacies that are interpreted to be deposited by two different types of sediment gravity flows: turbidity currents and transitional flows. Samples from beds that are taken from turbidites are finer and better sorted than those taken from hybrid beds (Figs. 8 C, D) and their deposition is controlled by different flow processes. We propose that deposits from a purely turbiditic succession would show a stronger fining trend, which is now dampened by the data from the hybrid bed deposits. It's clear that more work has to be conducted to study this longitudinal grain-size differentiation between the two flow types.

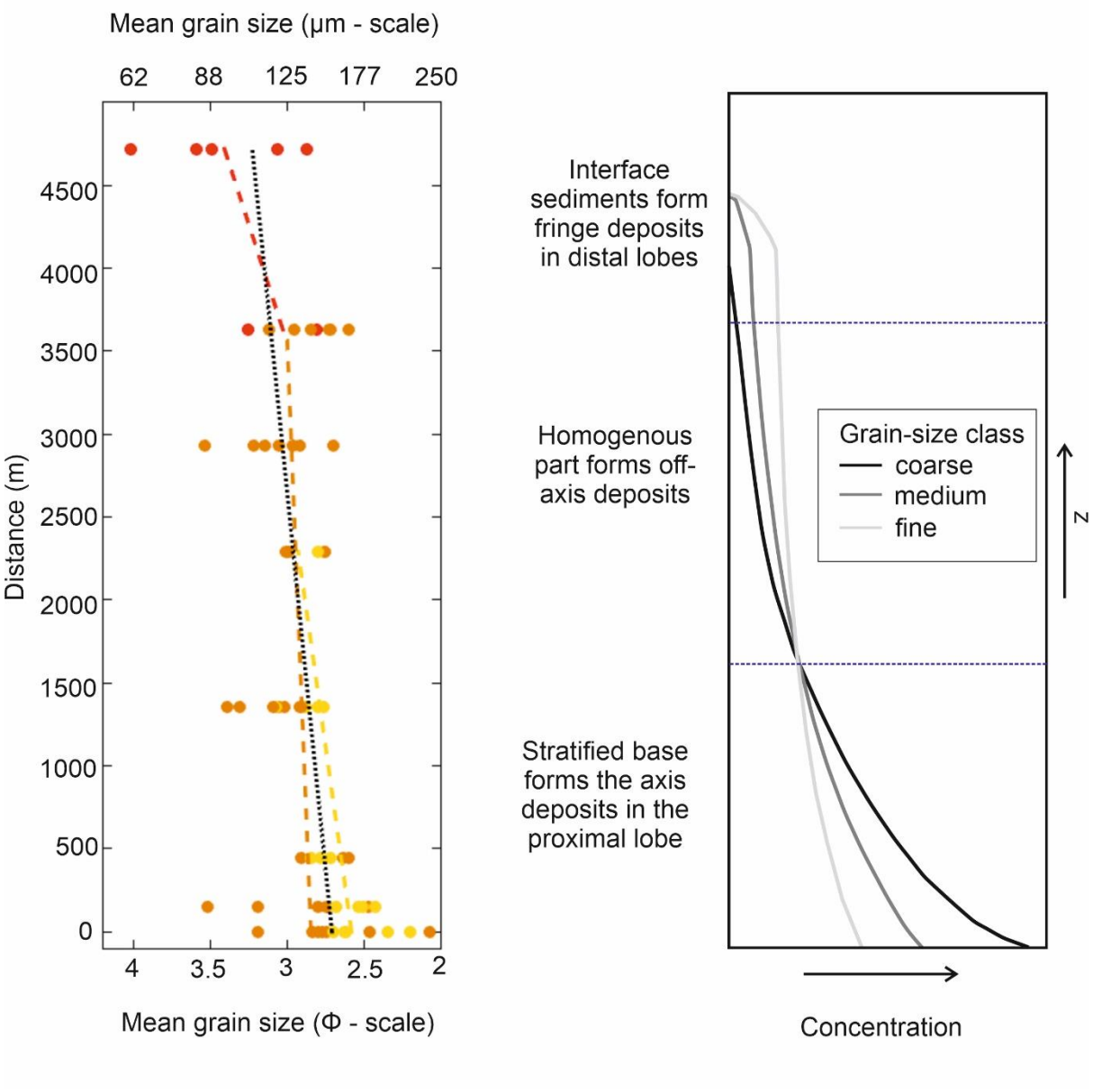

Fig. 13: Observed longitudinal evolution of grain-size distribution from the youngest lobe of Clinothem 12 compared with grain size concentration profiles for different grain size classes (after Eggenhuisen et al., 2020).

Expression of stacking patterns in grain size data

Lobe stacking patterns like progradation and retrogradation may skew the longitudinal grain-size distribution trend we see. While progradation would likely push the extend of coarse grain sizes further into the basin, retrogradation would cause a grain-size trend to finer material. In this case, we are confident that there is no major influence of progradational or retrogradational stacking patterns in our evaluation of the grain-size distributions for the youngest lobe of Clinothem 12. Neither vertical grain size distribution

(Fig. 11) nor bed thickness plots (Fig.14) for the individual logs are showing a clear coarsening and thickening upward trend, nor for a fining and thinning upward trend which would be characteristic of progradation and retrogradation, respectively.

However, it is likely that the influence of stacking patterns would become more apparent if analysis would be attempted for grainsize distributions for lobe complexes that comprise several lobes. Further work in a well reconstructed lobe complex example is necessary to assess this question.

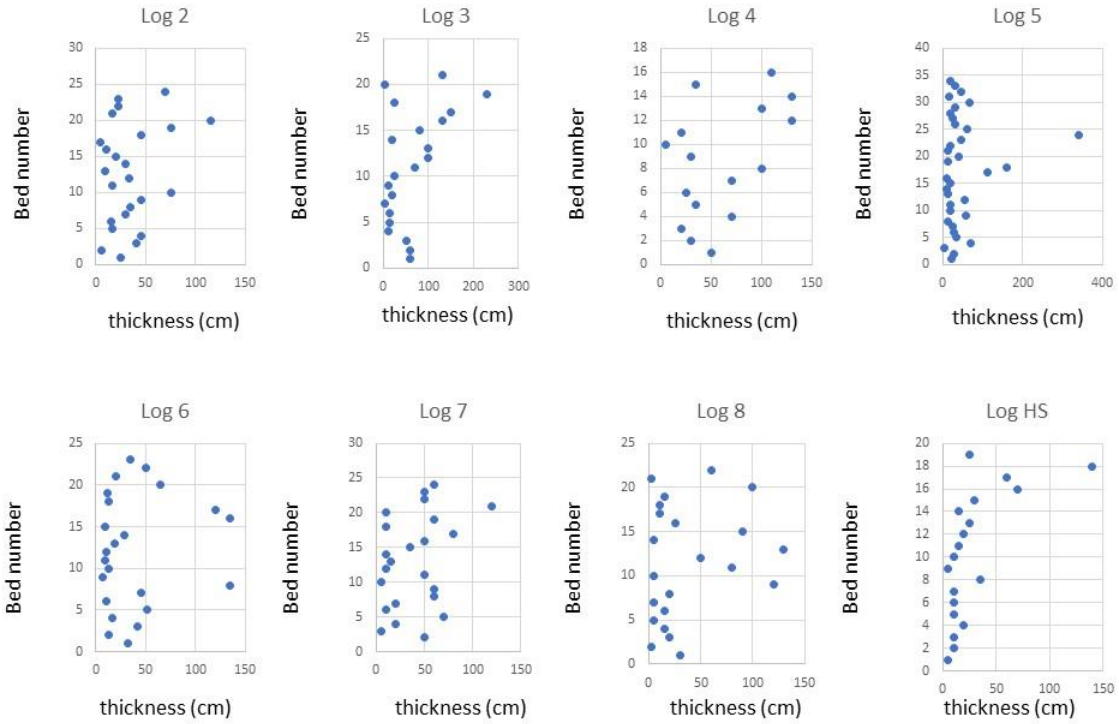

Fig. 14: Vertical bed thickness distribution for the individual logs of Clinothem 12. Note: Horizontal axis for Log 3 and Log 5 deviate from the other logs.

Implications for hydrocarbon reservoir quality

This study aims to understand how the spatial evolution of turbidity currents is recorded in lobe deposits on a scale of approximately 5 km. The results have implications for km-scale distribution of hydrocarbon reservoir parameters, as grain size is a main factor control on reservoir quality (Porten et al., 2016; Bell et al., 2018). The amalgamated structureless sandstones that characterise lobe-axis settings have been interpreted as high-density turbidity current deposits (Prélat et al., 2009; Grundvåg et al., 2014b; Spychala et al., 2017a; Bell et al., 2018). Generally, these deposits are associated with

the best reservoir characteristics as they are 1) commonly low on clay content which is connected to the highest permeabilities, and 2) have been suggested to have higher permeability because of their coarse grain size (Porten et al., 2016). Lobe off-axes are characterized by sediments that are deposited from high density turbidity currents as well as from low density turbidity currents. Bell et al. (2018) did not observe a significant change in sorting between lobe axis and off-axis, which conforms to observations from this study. However, besides finer grain size, the lobe off-axis is associated with an increase in matrix content which decreases permeability (Bell et al., 2018). Lobe fringe deposits comprise fine-grained deposits from low density turbidity currents and deposits that were deposited by flows that show turbulent as well as laminar behaviour (hybrid beds). Low density turbidites are associated with the finest grain sizes, highest matrix content and lowest net: gross. The results of our study suggest that reservoir quality changes with distance most strongly within lobe axis and lobe fringe, albeit in the case of lobe axis deposits the chance is from very high quality to high quality. The reservoir quality of lobe off-axis deposits is demonstrated to be homogenous without proximal to distal trends. This outcome has two implications: 1) It is justified to model lobes as high-quality reservoirs elements right until their transition to lobe fringes; and 2) Reservoir quality can be uncoupled from reservoir thickness as the intermediate lobe deposits show thinning without a change in depositional sand quality.

Conclusions

The basin-floor fans of the Battfjellet Formation in Svalbard that outcrop in a proximal to distal orientation create the rare opportunity to analyze the longitudinal evolution of these distal deposits from lobe axis to fringe over a distance of 5 km. Within the investigated basin floor segment of Clinothem 12, lobe sub-environments have been distinguished based on their characteristic lithofacies associations and bounding surfaces, which reflecting depositional flow properties. A transition from predominantly high-density turbidity current deposits to low-density turbidity current deposits and hybrid beds is observed. A total of 66 photographed thin-sections were manually counted to determine the grain-size distribution of lobe axis, lobe off-axis and lobe-fringe deposits. These sub-environments have statistically distinct and variable grain-size distributions superimposed on an overall non-linear fining trend from lobe axis to lobe fringe. Only a single sample yielded grain size results that could justify re-assignment of the macroscopic facies association that was ascribed *a priori* the thin section analysis. This success rate reinforces the confidence in established facies classification schemes for lobe deposits. Furthermore, the sub-environments show different longitudinal grain-size trends. Lobe axis and fringe settings show (weak) basinward fining trends whereas lobe off-axis

settings show no variation in grain-size distribution with distance. An explanation for these trends is the interplay of capacity driven deposition from the decelerating flow, the grain-size stratification of the flows, and advection of the flow over the lobe. Overall, the coarser grain-size fraction is enriched at the base of the flow and more prone to be deposited when capacity-driven deposition is evoked in the lobe axis. The lobe off-axis is suggested to be deposited from the more homogenously mixed part of the flow, whereas the lobe fringe is dominated by deposition of the upper parts of the flow, resulting in the sand pinch-out in the lobe fringe.

The implications of this study are multifaceted: 1) Grain-size stratification is an important factor of the evolution and deposition of turbidity currents over lobe deposits and may be incorporated into modelling approaches of lobe deposits; 2) lobes can be justifying modelled as high-quality bodies until their transition to lobe fringes; and 3) reservoir quality can be uncoupled from reservoir thickness as the intermediate lobe deposits show thinning but no change in depositional sand quality.

Acknowledgements

This project was funded by NWO (grant #NWO-ALW-Vidi-864.13.006), ExxonMobil, Shell, and Equinor for which we are thankful. Sten-Andreas Grundvåg received funding from the ARCEx project (Research Centre for Arctic Petroleum Exploration), which is funded by the Research Council of Norway (grant number 228107). Further, we would like to thank Captain Stig Henningsen of the MS Farm.

Literature

Bell, D., Kane, I. A., Pontén, A. S., Flint, S. S., Hodgson, D. M., & Barrett, B. J. (2018). Spatial variability in depositional reservoir quality of deep-water channel-fill and lobe deposits. Marine and Petroleum Geology, 98, 97-115.

Bergh, S. G., Braathen, A., & Andresen, A. (1997). Interaction of basement-involved and thin-skinned tectonism in the Tertiary fold-thrust belt of central Spitsbergen, Svalbard. AAPG bulletin, 81(4), 637-661

Boulesteix, K., Poyatos-Moré, M., Hodgson, D.M., Flint, S.S., Taylor, K.G. (2020) Fringe or background: Characterizing deep-water mudstones beyond the basin-floor fan sandstone pinchout. Journal of Sedimentary Geology, in press.

Bouma, A. H. (2000) Fine-grained, mud-rich turbidite systems: Model and comparison with coarse-grained, sand-rich systems. In: Fine-grained Turbidite Systems (Eds. Bouma, A. H. and Stone, C. G.), AAPG Memoir 72/SEPM Spec. Publ., 68, 9–19.

Braathen, A. and Bergh, S.G. (1995). Kinematics of Tertiary deformation in the basement-involved fold-thrust belt, western Nordenskiold Land, Svalbard: Tectonic implications based on fault slip data analysis. Tectonophysics, 249, 1−29.

Bruhn R. and Steel, R. (2003). High-Resolution Sequence Stratigraphy of a Clastic Foredeep Succession (Paleocene, Spitsbergen): An Example of Peripheral-Bulge-Controlled Depositional Architecture. Journal of Sedimentary Research, 73, 745-755.

Clark, B. E., and Steel, R. (2006). Eocene turbidite-population statistics from shelf edge to basin floor, Spitsbergen, Svalbard: Journal of Sedimentary Research, v. 76, p. 903– 918.

Crabaugh, J.P. and Steel, R.J. (2004) Basin-floor fans of the Central Tertiary Basin, Spitsbergen: relationship of basinfloor sand-bodies to prograding clinoforms in a structurally active basin. In: Confined Turbidite Systems (Eds S.A. Lomas and P. Joseph), Geol. Soc. London Spec. Publ., 222, 187–208.

de Leeuw, J., Eggenhuisen, J. T., Spychala, Y. T., Heijnen,M. S., Pohl, F. and Cartigny, M. J. B. (2018a) Sediment volume and grain-size partitioning between submarine channel-levee systems and lobes: An experimental study. J. Sed. Res., 88, 1–18.

de Leeuw, J., Eggenhuisen, J.T. and Cartigny, M.J.B. (2018),. Linking submarine channel–levee facies and architecture to flow structure of turbidity currents: insights from flume tank experiments. Sedimentology, 65, 931-951.

De Leeuw, J. (2017). The sedimentary record of submarine channel morphodynamics. PhD Thesis. Utrecht University. ISBN 978-90-6266-476-4.

Deptuck, M. E., Piper, D. J., Savoye, B., & Gervais, A. (2008). Dimensions and architecture of late Pleistocene submarine lobes off the northern margin of East Corsica. Sedimentology, 55(4), 869-898.

Eggenhuisen, J.T., Tilston, M.C., de Leeuw, J., Pohl, F., Cartigny, M.J.B. (2020). Turbulent diffusion modelling od sediment in turbidity currents: An experimental validation of the Rouse approach. Depositional Record 6, 203-216.

Etienne, S., Mulder, T., Bez, M., Desaubliaux, G., Kwasniewski, A., Parize, O., Dujoncquoy, E., and Salles, T. (2012). Multiple scale characterization of sand-rich distal lobe deposit variability: examples

from the Annot Sandstones Formation, Eocene–Oligocene, SE France: Sedimentary Geology, v. 273–274, p. 1–18.

Fildani, A., Clark, J., Covault, J.A., Power, B., Romans, B.W., Aiello, I.W. (2018). Muddy sand and sandy mud on the distal Mississippi fan: Implications for lobe depositional processes. Geosphere 14, 1051-1066.

Ganti, V., Lamb, M. P. and McElroy, B. (2014) Quantitative bounds on morphodynamics and implications for reading the sedimentary record. Nature Comm., 5, 3298.

Garcia, M.H. (1994) Depositional turbidity currents laden with poorly sorted sediment. Journal of Hydraulic Engineering 120, 1240-1263.

Grundvåg, S.-A., Helland-Hansen, W., Johannessen, E.P., Olsen, A.H. and Stene, S.A.K. (2014a) The depositional architecture and facies variability of shelf deltas in the Eocene Battfjellet Formation, Nathorst Land, Spitsbergen. Sedimentology, 61, 2172-2204.

Grundvåg, S.-A., Johannessen, E. P., Helland-Hansen, W., & Plink-Björklund, P. (2014b). Depositional architecture and evolution of progradationally stacked lobe complexes in the Eocene Central Basin of Spitsbergen. Sedimentology, 61, 535– 569. https://doi.org/10.1111/sed.12067

Hansen, L.A.S., Callow, R.H.T., Kane, I.A., Gamberi, F., Rovere, M., Cronin, B.T., Kneller, B. (2015). Genesis and character of thin-bedded turbidites associated with submarine channels. Marine and Petroleum Geology 67, 852-879.

Haremo, P., Andresen, A., & Dypvik, H. (1993). Mesozoic extension versus Tertiary compression along the Billefjorden Fault Zone south of Isfjorden, central Spitsbergen. Geological Magazine, 130(6), 783-795.

Haughton, P. D. (1994). Deposits of deflected and ponded turbidity currents, Sorbas Basin, Southeast Spain. Journal of sedimentary Research, 64(2a), 233-246.

Helland-Hansen, W. & Grundvåg, S.-A., (2020) The Svalbard Eocene-Oligocene (?) Central Basin succession: Sedimentation patterns and controls. Basin Research.

Helland-Hansen, W. (1992). Geometry and facies of Tertiary clinothems, Spitsbergen. Sedimentology, 39, 1013-1029.

Helland-Hansen, W. (1990) Sedimentation in Paleogene foreland basin, Spitsbergen. AAPG Bull., 74, 260-272.

Hiscott, R.N., Hall, F.R., Pirmez, C. (1997). Turbidity-current overspill from the Amazon Channel: texture of the silt/sand load, paleoflow from anisotropy of magnetic susceptibility and implications for flow processes. Proceedings of the Ocean Drilling Program, Scientific Results 155, 53-78.

Hiscott, R.N., (1994). Loss of capacity, not competence, as the fundamental process governing deposition from turbidity currents. Journal of Sedimentary Research 64, 209-214.

Hubbard, S.M., Covault, J.A., Fildani, A., and Romans, B.W. (2014). Sediment transfer and deposition in slope channels: deciphering the record of enigmatic deep-sea processes from outcrop: Geological Society of America, Bulletin, v. 126, p. 857–871

Jobe, Z., Z. Sylvester, M. B. Pittaluga, A. Frascati, C. Pirmez, D. Minisini, N. Howes, and A. Cantelli (2017), Facies architecture of submarine channel deposits on the western Niger Delta slope: Implications for grain-size and density stratification in turbidity currents, J. Geophys. Res. Earth Surf., 122, 473–491.

Johannessen, E.P. and Steel, R.J. (2005) Shelf-margin clinoforms and prediction of deepwater sands. Basin Research, 17, 521-550.

Kane, I.A., Clare, M.A. (2019) Dispersion, Accumulation, and the Ultimate Fate of Microplastics in Deep-Marine Environments: A Review and Future Directions. *Front. Earth Sci.* 7:80. doi: 10.3389/feart.2019.00080

Kane, I. A., Pontén, A. S., Vangdal, B., Eggenhuisen, J. T., Hodgson, D. M., & Spychala, Y. T. (2017). The stratigraphic record and processes of turbidity current transformation across deep-marine lobes. Sedimentology, 64(5), 1236-1273.

Kellogg, H.E. (1975). Tertiary stratigraphy and tectonism in Svalbard and continental drift. American Association of Petroleum Geologists Bulletin, 59, 465-485.

Kneller, B., Buckee, C. (2000). The structure and fluid mechanics of turbidity currents: a review of some recent studies and their geological implications. Sedimentology 47, 62-94.

Kneller, B., and McCaffrey, W. (1999). Depositional effects of flow nonuniformity and stratification within turbidity currents approaching a bounding slope; deflection, reflection and facies variation. Journal of Sedimentary Research 69, 980-991.

Kneller, B., Edwards, D., McCaffrey, W., & Moore, R. (1991). Oblique reflection of turbidity currents. Geology, 19(3), 250-252.

Kranck, K. (1984). Grain-size characteristics of turbidites. Geological Society, London, Special Publications, 15(1), 83-92.

Leever, K. A., Gabrielsen, R. H., Faleide, J. I., & Braathen, A. (2011). A transpressional origin for the West Spitsbergen fold-and-thrust belt: Insight from analog modeling. Tectonics, 30(2), 1-24

Lundin, E. & Doré, A. (2002). Mid-Cenozoic post-breakup deformation in the 'passive'margins bordering the Norwegian–Greenland Sea. Marine and Petroleum Geology, 19, 79-93.

Marchand, A.M.E., Apps, G., Li, W., and Rotzien, J.R. (2015). Depositional processes and impact on reservoir quality in deepwater Paleogene reservoirs, US Gulf of Mexico: American Association of Petroleum Geologists, Bulletin, v. 99, p. 1635–1648.

Masalimova, L.U., Lowe, D.R., Sharman, G.R., King, P.R., and Arnot, M.J. (2016). Outcrop characterization of a submarine channel–lobe complex: the Lower Mount Messenger Formation, Taranaki Basin, New Zealand: Marine and Petroleum Geology, v.71, p. 360–390.

Mellere, D., Plink-Björklund, P. and Steel, R.J. (2002) Anatomy of shelf deltas at the edge of a prograding Eocene shelf margin, Spitsbergen. Sedimentology, 49, 1181–1206

Müller, R.D. and Spielhagen, R.F. (1990) Evolution of the Central Tertiary Basin of Spitsbergen: towards a synthesis of sediment and plate tectonic history. Palaeogeogr. Palaeoclimatol. Palaeoecol., 80, 153–172.

Myhre, A. M., Eldholm, O., & Sundvor, E. (1982). The margin between Senja and Spitsbergen fracture zones: implications from plate tectonics. Tectonophysics, 89(1-3), 33-50.

Paola, C. and Martin, J.M. (2012). Mass-balance effects in depositional systems. Journal of Sedimentary Research 82, 435-450.

Petersen, T.G., Thomsen, T., Olaussen, S. and Stemmerik, L. (2016) Provenance shifts in an evolving Eurekan foreland basin: the Tertiary Central Basin, Spitsbergen. J. Geol. Soc., 173, 634-648.

Piepjohn, K., von Gosen, W. & Tessensohn, F. (2016). The Eurekan deformation in the Arctic: an outline. Journal of the Geological Society, 173, 1007-1024.

Pirmez, C., Imran, J. (2003). Reconstruction of turbidity currents in the Amazon Channel. Marine and Petroleum Geology 20, 823-849.

Plink-Björklund, P., Mellere, D. and Steel, R.J. (2001) Turbidite variability and architecture of sand-prone, deepwater slopes: Eocene clinoforms in the Central Basin, Spitsbergen. J. Sed. Res., 71, 895–912.

Pohl, F., Eggehuisen, J.T., Kane, I.A., Clare, M.A. (2020) Transport and Burial of Microplastics in Deep-Marine Sediments by Turbidity Currents. *Environ. Sci. Technol.* 54, 7, 4180–4189

Pohl, F., & T. McCann, (2014). Architecture and depositional development of the Eocene deep-marine Morillo and Coscojuela Formations, Aínsa Basin, Spain: Geological Journal, v. 49, no. 3, p. 221–238.

Porten, K. W., Kane, I. A., Warchoł, M. J., & Southern, S. J. (2016). A sedimentological process-based approach to depositional reservoir quality of deep-marine sandstones: an example from the Springar Formation, northwestern Vøring Basin, Norwegian Sea. Journal of Sedimentary Research, 86(11), 1269-1286.

Prather, B. E., O'Byrne, C., Pirmez, C., & Sylvester, Z. (2017). Sediment partitioning, continental slopes and base-of-slope systems. Basin Research, 29(3), 394-416.

Prélat, A., and Hodgson, D.M. (2013). The full range of turbidite bed thickness patterns in submarine lobes: controls and implications: Geological Society of London, Journal, v.170, p. 1–6.

Prélat, A. Hodgson, D. & Flint, S. (2009). Evolution, architecture and hierarchy of distributary deep-water deposits: a high-resolution outcrop investigation from the Permian Karoo Basin, South Africa. Sedimentology, 56, 2132-2154.

Spotts, J. H. (1964). Grain orientation and imbrication in Miocene turbidity current sandstones, California. Journal of Sedimentary Research, 34(2), 229-253.

Spychala, Y.T., Eggenhuisen, J.T., Tilston, M., Pohl, F. (2020) The influence of basin setting and turbidity current properties on the dimensions of submarine lobe elements. Sedimentology. doi: 10.1111/sed.12751

Spychala, Y. T., Hodgson, D. M., Prélat, A., Kane, I. A., Flint, S. S., & Mountney, N. P. (2017a). Frontal and lateral submarine lobe fringes: comparing sedimentary facies, architecture and flow processes. Journal of Sedimentary Research, 87(1), 75-96.

Spychala, Y.T., Hodgson, D.M., Lee, D.R. (2017b). Autogenic controls on hybrid bed distribution in submarine lobe complexes. Marine and Petroleum Geology 88, 1078-1093.

Spychala, Y.T., Hodgson, D.M., Flint, S.S., and Mountney, N.P. (2015). Constraining the sedimentology and stratigraphy of submarine intraslope lobe deposits using exhumed examples from the Karoo Basin, South Africa: Sedimentary Geology, v. 322, p. 67–81.

Steel, R.J. and Olsen, T. (2002) Clinoforms, clinoform trajectories and deepwater sands. In: Sequence Stratigraphic Models for Exploration and Production: Evolving Methodology, Emerging Models and Application Histories (Eds J.M. Armentrout and N.C. Rosen), GCS-SEPM Found 22nd Annu Res Conf Proc, 367–381 (CD-ROM).

Steel, R., Gjelberg, J., Helland-Hansen, W., Kleinspehn, K., Nøttvedt, A. & Rye-Larsen, M. (1985). The Tertiary strike-slip basins and orogenic belt of Spitsbergen. SEPM Special Publication, 37, 339-359.

Steel, R., Dalland, A., Kalgraff, K. and Larsen, V. (1981) The Central Tertiary Basin of Spitsbergen: sedimentary development of a Sheared-Margin Basin. In: Geology of the North Atlantic Borderland (Eds J.W. Kerr and A.J. Ferguson), Can. Soc. Petrol. Geol. Mem., 7, 647-664.

Stevenson, C. J., Talling, P. J., Sumner, E. J., Masson, D. G., Frenz, M., & Wynn, R. B. (2014b). On how thin submarine flows transported large volumes of sand for hundreds of kilometres across a flat basin plain without eroding the sea floor. Sedimentology, 61(7), 1982-2019.

Straub, K.M., Mohrig, D., and Pirmez, C., 2012, Architecture of an aggradational tributary submarine channel network on the continental slope offshore Brunei Darussalam, in Prather, B.E., Deptuck, M.E., Mohrig, D.C., vanHoorn, B., and Wynn, R.B., eds., Application of the Principles of Seismic Geomorphology to Continental-Slope and Base-of-Slope Systems: Case Studies From Seafloor and Near-Seafloor Analogues: SEPM, Special Publication 99, p. 145–161.

Sylvester, Z., & Lowe, D. R. (2004). Textural trends in turbidites and slurry beds from the Oligocene flysch of the East Carpathians, Romania. Sedimentology, 51(5), 945-972.

Tilston, M., Arnott, R.W.C., Rennie, C.D., Long, B. (2015). The influence of grain size on the velocity and sediment concentration profiles and depositional record of turbidity currents. Geology 43, 839-842.

van der Merwe, W.C., Hodgson, D.M., Brunt, R.L., AND Flint, S.S., 2014, Depositional architecture of sand-attached and sand-detached channel–lobe transition zones on an exhumed stepped slope mapped over a 2500 km2 area: Geosphere, v. 10, p. 1076–1093

Tables

Table 1. Observed lithofacies in Clinothem 12, their processes and depositional environment

Figures

Figure 1: A) Location of the Central Tertiary Basin (CTB). The square indicates the location of the study area in the Van Keulenfjorden. B) Stratigrpahy of the CTB (modified from Crabaugh and Steel, 2004). The Battfjellet Formation is interpreted to be of an Eocene to possible Oligocene age. C: Location of outcrop sections along Storvola and Hyrnestabben used in the study. Satellite images are taken from Google Earth.

Figure 2: Correlation panel of Clinothem 12. Uncertain correlations are pointed out with dashed black lines. Red lines indicate erosion surfaces. The normal fault between log 5 and log 6 is marked by a dark blue line.

Fig. 3: Locations of samples and sample number taken within the deposits of the youngest lobe. Colours indicate the interpreted lobe sub-environment from field data alone.

Figure 4: A) Photo panel of the study area with Storvola in the foreground and Hyrnestabben in the background to the right. Log locations are indicated with their numbers. B) Example of F1: structureless sandstone. Lens cover for scale (~ 7 cm diameter). C) Example of F2: planar laminated sandstone. Folded rule (20 cm) as scale. D) Example of F3: Structured sandstone. Here the deposit shows ripple laminations. Lens cover for scale (~ 7 cm diameter). E) The log section at Hyrnestabben (Log HS) shows F6 (siltstones) at its base which are overlain by F4 (heterolithic interval). Geological hammer (30 cm) for scale. F) Folded sandstones at the base of the youngest lobe in the section of Log 7. Rule (100 cm) for scale. G) Hybrid bed (F5) at Log HS. Note the irregular transition from clean sandstone to the debritic division which is weathered back into the slope. Folded rule (20 cm) for scale.

Figure 5: A) Simplified model indicating the various sub-environments in a lobe (redrawn from Prélat et al. 2009). B) Plan-form view of five-fold lobe hierarchy: bed to bed set, lobe element, lobe, lobe complex, and lobe complex set (modified from Prélat et al. 2010, redrawn from Spychala et al., 2017a).

Figure 6: Rose diagram of vertical orientation of grains of all the samples. The area of each bar is the relative number of observations.

Figure 7: Probability density functions of the grain-size distributions of basin-floor fan deposits of Clinothem 12 showing all 66 grain-size distributions of lobe axis (yellow), off-axis (orange), and fringe (red) samples.

Figure 8: Longitudinal development of mean grain-size. Black dotted line indicates the linear regression of the mean grain-size of all samples with longitudinal distance (R2 = 0.27). Lobe axis, off-axis and fringe samples and their linear regression with distance (R2 = 0.33, R2 = 0.04, R2 = 0.18, respectively) are indicates by the yellow, orange, and red points and dotted lines, respectively. Note the relative stable range in mean grain-size of lobe off-axis samples.

Figure 9: Boxplots of grain-size distributions in vertical succession (with 1 referring to the lowermost sample up to highest sample within the log) of individual logs. Colours indicate the sub-environments lobe axis (yellow), off-axis (orange), and fringe (red). The vertical line within the box indicates the median and the boundaries of the box indicate the 25th and 75th percentile. The whiskers, marked as ⊦ - -, extend 1.5 times the interquartile distance (distance between indicate the 25th and 75th percentile). The plotted whiskers extend up to adjacent value that is the most extreme data point within the calculated whisker. The outlier, marked as +, are values above or below the whiskers.

Figure 10: Examples of lobe sub-environment lithology and grain size in thin-sections. A) Lobe axis. Sample 6 of Log 3. B) Lobe off-axis. Sample 12 of Log 5. C) Lobe fringe. Sample 4 of Log Hs. D) Lobe fringe hybrid bed. Sample 8 of Log HS.

Figure 11: Probability density functions of the grain-size distributions of lobe sub-environment deposits of Clinothem 12. A) Lobe axis. B) Lobe off-axis. C) Lobe fringe.

Figure 12: A) Geometry and general distribution of lobe sub-environments. B) Longitudinal grain size evolution of lobe deposits. The old linear model is indicated in a blue dashed line, whereas the non-linear trend suggested by this study is indicated by a pink solid line.